Journal of Organometallic Chemistry 1046 (2026) 123999

Contents lists available at ScienceDirect

Journal of Organometallic Chemistry

journal homepage: www.elsevier.com/locate/jorganchem

Testing cuprophilicity with tetrahedral ruthenium hydride carbonyl clusters☆

Cristiana Cesari [a,*], Marco Bortoluzzi [b], Cristina Femoni [a], Francesca Forti [a], Maria Carmela Iapalucci [a], Giorgia Scorzoni [a], Stefano Zacchini [a,*]

[a] Dipartimento di Chimica Industriale "Toso Montanari", Università di Bologna, Via P. Gobetti, Bologna 85-40129, Italy
[b] Dipartimento di Scienze Molecolari e Nanosistemi, Ca' Foscari University of Venice, Via Torino, Mestre, Venice 155-30175, Italy

ARTICLE INFO

Keywords:
Cluster compounds
Carbonyl ligands
Cuprophilic interactions
Computational investigations
Heterometallic bonds

ABSTRACT

The reaction of $[NEt_4]_3$ $[HRu_4(CO)_{12}]$ (**1**) with three mole equivalents of $[Cu(MeCN)_4][BF_4]$ and three mole equivalents of $[NEt_4]Br$ affords a nearly 1:1 mixture of $[NEt_4]_3$ $[HRu_4(CO)_{12}(CuBr)_3]$ (**2**) and $[NEt_4]_2$ $[H_2Ru_8(CO)_{24}Cu_7Br_3]$ (**3**). These two products can be separated owing to their different solubilities in organic solvents. $[NEt_4]_3$ $[HRu_8(CO)_{24}Cu_6Br_2]$ (**4**) has been obtained reacting **1**, $[Cu(MeCN)_4][BF_4]$ and $[NEt_4]Br$ with stoichiometry 1:1:3. In the absence of $[NEt_4]Br$, **1** reacts with 3.5 mole equivalents of $[Cu(MeCN)_4][BF_4]$ affording $[Ru_5(CO)_{15}(CuMeCN)_2]$ (**5**). The new clusters **2**–**5** have been fully characterized by FT-IR and ^1H NMR spectroscopy, and their molecular structures elucidated by single-crystal X-ray diffraction (SC-XRD). Homometallic Ru-Ru and Cu-Cu as well as heterometallic Ru-Cu interactions have been computationally investigated by DFT methods.

1. Introduction

Even though metallophilic interactions are well-established nowadays, several experimental and theoretical studies are still ongoing to fully understand their nature [1–5]. Metallophilicity is claimed to be important for structural control, catalysis, luminescence and sensing applications [6]. The most studied sub-class of metallophilic interactions are aurophilic interactions, which involve d^{10} Au^+ centers [7–9]. Metallophilicity has been reported also for other closed shell d^{10} centers (e.g., Cu^+, Ag^+, Hg^{2+}) and pseudo-closed shell d^8 centers (e.g., Pd^{2+}, Pt^{2+}) [10–13]. Metallophilic interactions result from a combination of covalency (sp or spd orbital hybridization), London dispersion forces, electron correlation effects, relativistic effects, dispersion forces, closed shell Pauli repulsion, and may (or may not) be further supported by multidentate ligands [14]. The relative importance of these different components is still under investigation, and further experimental examples should be examined. Cuprophilicity has been so far less investigated than aurophilicity, even though more examples have been recently added [15–17].

As in the case of other weak forces [18,19], metallophilic interactions operate both inter- and intra-molecularly. At the inter-molecular level, such weak forces, including metallophilicity, are fundamental in supramolecular chemistry. Intra-molecularly, they contribute to the overall structure and chemical reactivity of a molecule. We have previously shown that surface decorated metal carbonyl clusters (MCCs) are suitable platforms to test intra-molecular weak metallophilic interactions [20]. This particularly applies to aurophilicity and, indeed, several MCCs decorated on the surface by Au(I)-fragments have been reported [21–27]. Mercurophilic interactions in MCCs have also been discussed recently [28].

MCCs have largely contributed to Cotton's definition of metal clusters and to a better understanding of metal-metal bonding in molecular clusters [29–36]. Both homometallic and heterometallic MCCs have been investigated at a fundamental level, and for applicative purposes, especially in catalysis [37–39]. Most Ru-Cu MCCs reported to date may be viewed as homometallic Ru MCC anions interacting with Cu(I)-based

☆ Dedicated to Professor Richard D. Adams celebrating his contribution to organometallic and cluster chemistry on the occasion of his retirement as Editor-in-Chief for the Journal of Organometallic Chemistry.

* Corresponding authors.
E-mail addresses: cristiana.cesari2@unibo.it (C. Cesari), stefano.zacchini@unibo.it (S. Zacchini).

https://doi.org/10.1016/j.jorganchem.2025.123999
Received 17 November 2025; Received in revised form 22 December 2025; Accepted 26 December 2025
Available online 29 December 2025

fragments [40–44]. When two or more Cu(I) centers are present, sub van der Waals Cu···Cu contacts are often present, suggesting the presence of cuprophilic interactions. Thus, Ru-Cu MCCs may be used to investigate cuprophilicity at an intra-molecular level. Moreover, Ru-Cu MCCs have been used for the preparation of polymers, bimetallic nanoparticles and nanostructured heterogeneous catalysts [45–47].

Herein, we report the synthesis of four new heterometallic Ru-Cu MCCs, their structural characterization by single-crystal X-ray diffraction (SC-XRD) and a computational analysis of their metal-metal bonding.

2. Results and discussion

2.1. Synthesis

Different products can be obtained from the reactions between $[NEt_4]_3[HRu_4(CO)_{12}]$ (**1**) and $[Cu(MeCN)_4][BF_4]$, depending on stoichiometry and the amount of $[NEt_4]Br$ added to the reaction mixture (Scheme 1). A bromide source seems to be necessary to avoid oxidation of **1** and, thus, the species $[NEt_4]_3[HRu_4(CO)_{12}(CuBr)_3]$ (**2**), $[NEt_4]_2[H_2Ru_8(CO)_{24}Cu_7Br_3]$ (**3**), and $[NEt_4]_3[HRu_8(CO)_{24}Cu_6Br_2]$ (**4**) have been isolated performing the reactions in the presence of $[NEt_4]Br$. In detail, a mixture of **2** and **3** is obtained using three moles of $[Cu(MeCN)_4][BF_4]$ and three moles of $[NEt_4]Br$ per mole of **1**. Clusters **2** and **3** may be separated by solvent extraction, since **3** is soluble in CH_2Cl_2 and **2** in acetone. Cluster **4** may be prepared using a decreased amount of $[Cu(MeCN)_4][BF_4]$ in the presence of $[NEt_4]Br$. Compound **4** can be transformed into a mixture of **2** and **3** upon a further addition of $[Cu(MeCN)_4][BF_4]$ in the presence of $[NEt_4]Br$ Fig. 1.

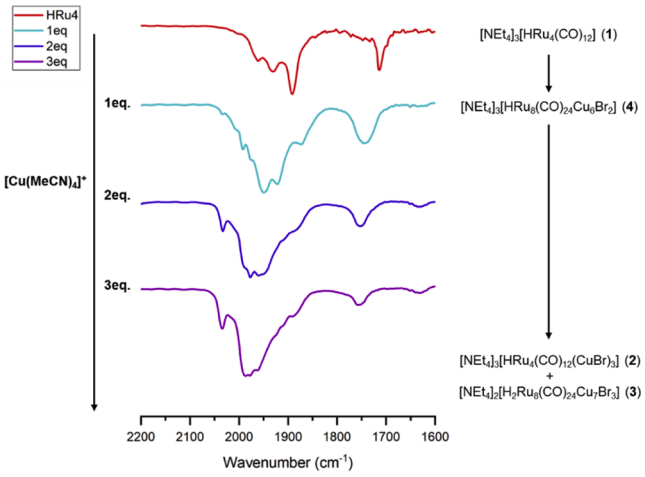

Fig. 1. IR spectra in the ν_{CO} region of the stepwise addition of $[Cu(MeCN)_4][BF_4]$ to a solution of 1 and $[NEt_4]Br$ in MeCN.

In contrast, in the absence of $[NEt_4]Br$, $[Cu(MeCN)_4][BF_4]$ partially oxidizes **1** affording mixtures of products, among which the new $[Ru_5(CO)_{15}(CuMeCN)_2]$ (**5**) cluster has been isolated in moderate yields, using 3.5 mol of $[Cu(MeCN)_4][BF_4]$ per mole of **1**.

It must be remarked that performing the reactions of **1** with $[Cu(MeCN)_4][BF_4]$ in the presence of less than three moles of $[NEt_4]Br$ per mole of **1**, complex mixtures of products are obtained. For instance, using two moles of $[Cu(MeCN)_4][BF_4]$ per mole of **1** in the presence of one mole of $[NEt_4]Br$, the previously reported $[NEt_4]_2[Ru_8(CO)_{26}Cu_2]$

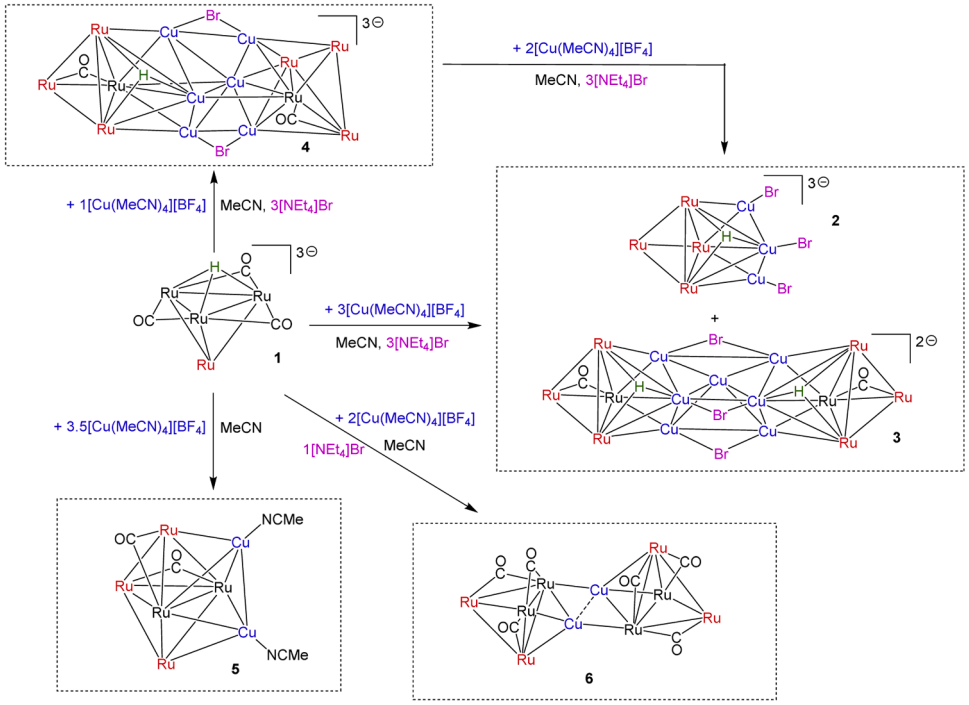

Scheme 1. Synthesis of 2–**5.** $[Ru_3(CO)_{12}]$ (**7**) has been observed sometimes as side-product, especially when using an excess of $[Cu(MeCN)_4][BF_4]$ and/or in the absence of $[NEt_4]Br$. Terminal CO ligands have been omitted for clarity. Ru atoms represented in red are bonded to three terminal carbonyls, those represented in black are bonded to two terminal carbonyls.

$$[HRu_4(CO)_{12}]^{3-} + 3Cu^+ + 3Br^- \rightleftharpoons [HRu_4(CO)_{12}(CuBr)_3]^{3-} \quad (1)$$
1 **2**

$$2[HRu_4(CO)_{12}]^{3-} + 7Cu^+ + 3Br^- \rightleftharpoons [H_2Ru_8(CO)_{24}Cu_7Br_3]^{2-} \quad (2)$$
1 **3**

$$2[HRu_4(CO)_{12}]^{3-} + 6Cu^+ + 2Br^- \rightleftharpoons [HRu_8(CO)_{24}Cu_6Br_2]^{2-} + H^+ \quad (3)$$
1 **4**

$$[H_2Ru_8(CO)_{24}Cu_7Br_3]^{2-} + 3Br^- \rightleftharpoons 2[HRu_4(CO)_{12}(CuBr)_3]^{3-} + Cu^+ \quad (4)$$
3 **2**

$$[HRu_8(CO)_{24}Cu_6Br_2]^{2-} + H^+ + Cu^+ + Br^- \rightleftharpoons [H_2Ru_8(CO)_{24}Cu_7Br_3]^{2-} \quad (5)$$
4 **3**

$$H^+ + Br^- \rightleftharpoons HBr \quad (6)$$

$$H_2O + Cu^+ \rightleftharpoons H^+ + CuOH \quad (7)$$

Scheme 2. Lewis and Bronstead type equilibria involved in the synthesis of **2**–**4**.

(**6**) cluster has been isolated [44]. Sometimes $[Ru_3(CO)_{12}]$ (**7**) has been spectroscopically observed as a side-product, especially when using an excess of $[Cu(MeCN)_4][BF_4]$ and/or in the absence of $[NEt_4]Br$.

The new species **2**–**5** have been fully characterized by FT-IR and ^1H NMR spectroscopy (Figs. S1-S22 in the Supporting Information), and their molecular structures elucidated by SC-XRD.

As well described in the literature, owing to the π-acidic character of CO ligands, hydrides in metal carbonyl compounds possess a slight acidic character and may be viewed as protons, H^+ [34]. Thus, considering CO as a neutral ligand, the formal oxidation state of Ru in **1** is −1. Formation of compounds **2**–**4** may be viewed as the result of condensation equilibria (Lewis type acid-base reactions) involving **1**, Cu^+ and Br^- ions, as those depicted in reactions (1)-(5) of Scheme 2. Bromides may also act as Bronstead bases *via* equation (6), whereas protons may be generated by hydrolysis of traces of moisture, also promoted by Cu^+ ions (7). The formal oxidation of Ru in all compounds **2**–**4** is −1, as in 1. The positions of the different equilibria depend on the concentrations of the species involved.

Assuming that Cu retains the +1 oxidation state in all the clusters, the formal oxidation state of Ru in **5, 6**, and **7** is −0.4, −0.5 and 0, respectively. Thus, their formation from **1** involves formal oxidation of Ru (Scheme 3). The oxidant is likely to be Cu^+, whose oxidizing power is greater in the absence of Br^- ions.

2.2. Molecular structures and computational studies

2.2.1. $[HRu_4(CO)_{12}(CuBr)_3]^{3-}$ (2)

Cluster **2** may be viewed as a $[HRu_4(CO)_{12}]^{3-}$ tetrahedral cluster decorated by three CuBr fragments (Figs. 2 and 3; Table S1 in the Supporting Information). Cu1 is capping one triangular face of the Ru_4 tetrahedron, resulting in a Ru_4Cu trigonal bipyramid. Cu2 and Cu3 are μ_3-coordinated to two Ru_2Cu faces of such trigonal bipyramid. A similar Ru_4M_3 core has been previously found in $[HRu_4(CO)_{12}(AuPPh_3)_3]$ (isomer A) [48,49], $Ru_3Co(CO)_{12}(AuPPh_3)_3$, [50], and $[H_2Ru_8(CO)_{24}Cu_7Cl_3]^{2-}$ [41].

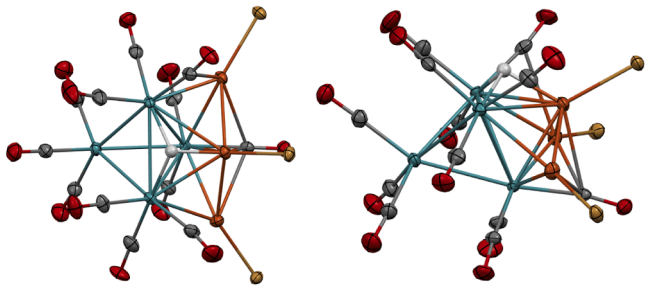

Fig. 2. Two views of the molecular structure of **2** (turquoise, Ru; orange, Cu; brown, Br; red O; grey C; white H).

The unique hydride of **2** has been preliminarily located by SC-XRD and then, its position corroborated by DFT calculations. H1 is capping the Ru_2Cu face of the Ru_4Cu trigonal bipyramid which is not capped by the other two Cu atoms. The computed Ru-H distances after optimization of the hydride position by means of periodic DFT calculations on the cesium salt of **2** are equal to 1.829 and 1.846 Å, while the computed Cu-H bond length is 1.836 Å. The μ_3 coordination mode of the hydride has also been confirmed by full DFT optimization of the anion **2** with the r^{2}SCAN-3c DFT method (Ru-H 1.841 and 1.847 Å, Cu-H 1.883 Å) [51]. It is noteworthy that in the above mentioned isomer of $[HRu_4(CO)_{12}(AuPPh_3)_3]$ [49] presenting the same Ru_4M_3 core of **2**, the hydride

$$2[HRu_4(CO)_{12}]^{3-} + 6Cu^+ + 3CO \rightleftharpoons [Ru_5(CO)_{15}(CuMeCN)_2] + [Ru_3(CO)_{12}] + H_2 \quad (8)$$
1 **5** **7**

$$2[HRu_4(CO)_{12}]^{3-} + 4Cu^+ + 2CO \rightleftharpoons [Ru_8(CO)_{26}Cu_2]^{2-} + H_2 + 2Cu \quad (9)$$
1 **6**

$$5[HRu_4(CO)_{12}]^{3-} + 15Cu^+ \rightleftharpoons 4[Ru_5(CO)_{15}(CuMeCN)_2] + 2.5H_2 + 7Cu \quad (10)$$
1 **5**

$$3[HRu_4(CO)_{12}]^{3-} + 9Cu^+ + 12CO \rightleftharpoons 4[Ru_3(CO)_{12}] + 1.5H_2 + 9Cu \quad (11)$$
1 **7**

Scheme 3. Representative redox reactions likely involved in the formation of **5**–**7**.

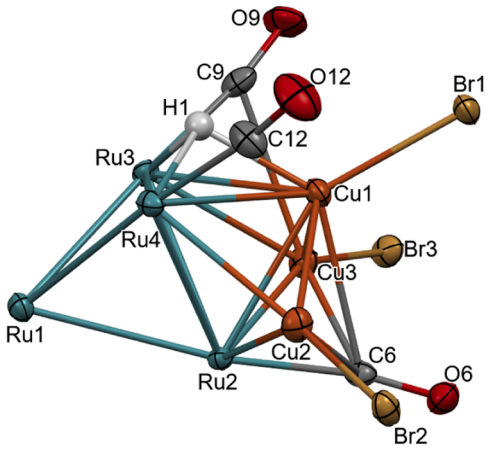

Fig. 3. Labelling scheme of **2** (turquoise, Ru; orange, Cu; brown, Br; red O; grey C; white H). Terminal CO ligands are not represented for clarity.

Table 1
Selected properties at Ru-Ru, Ru-H, Ru-Cu, Cu-H, Cu-Cu and Cu-C BCPs for 2.

Attractors	ρ (a.u.)	V (a.u.)	E (a.u.)	$\nabla^2\rho$(a.u.)
Ru1-Ru2	0.0459	−0.0343	−0.0115	0.0454
Ru1-Ru3	0.0455	−0.0331	−0.0114	0.0415
Ru1-Ru4	0.0448	−0.0328	−0.0110	0.0431
Ru2-Ru3	0.0406	−0.0287	−0.0090	0.0429
Ru2-Ru4	0.0407	−0.0288	−0.0091	0.0429
Ru3-H	0.0736	−0.0823	−0.0213	0.1587
Ru4-H	0.0743	−0.0839	−0.0217	0.1616
Cu1-H	0.0537	−0.0543	−0.0113	0.1271
Ru2-Cu1	0.0409	−0.0329	−0.0079	0.0681
Ru2-Cu2	0.0420	−0.0333	−0.0087	0.0637
Ru2-Cu3	0.0428	−0.0353	−0.0087	0.0713
Ru3-Cu3	0.0442	−0.0364	−0.0093	0.0712
Cu2-C12	0.0590	−0.0564	−0.0104	0.1425
Cu3-C6	0.0413	−0.0329	−0.0040	0.0995
Cu1-Cu2	0.0364	−0.0286	−0.0061	0.0651
Cu1-Cu3	0.0359	−0.0277	−0.0062	0.0610

ligand was located on a Ru_3 triangular face. This is somehow related to the higher tendency of Cu compared to Au to form hydrides [52–54]. Indeed, a few other Ru-Cu clusters containing a Ru_4Cu trigonal bipyramidal core whose three Ru_2Cu triangular faces are all capped by hydrides or Cu fragments are known, that is, $[H_2Ru_4(CO)_{12}(CuPPh_3)_2]$ [55], $[H_2Ru_4(CO)_{12}\{Cu_2(P\text{-}P)\}]$ (P-*P* = $Ph_2P(CH_2)_2PPh_2$, $Ph_2P(CH_2)_3PPh_2$, $Ph_2P(CH_2)_5PPh_2$) [56], $H_2Ru_4(CO)_{12}\{Cu_2(dppf)\}]$ (dppf = $Fe(\eta^5\text{-}C_5H_4PPh_2)_2$) [57], $[H_3Ru_4(CO)_{12}(CuPMePh_2)]$ [58], $[H_3Ru_4(CO)_{12}(CuMeCN)]$ [43], and $[\{H_3Ru_4(CO)_{12}Cu\}_2\{Ph_2P(CH_2)_2PPh_2\}]$ [59].

Within the six Ru-Ru bonds, the three ones not spanned by a hydride or Cu fragment [Ru1-Ru2 2.8008(5) Å, Ru1-Ru3 2.7873(5) Å, Ru1-Ru4 2.7901(5) Å] are significantly shorter than the other three [Ru2-Ru3 2.9067(5) Å, Ru2-Ru4 2.9537(5) Å, Ru3-Ru4 2.9430(5) Å]. Selected bonds in the DFT-optimized structure of **2** have been investigated by means of the Atoms-in-Molecules (AIM) analysis (see Table 1 and Fig. 4). Five Ru-Ru (3,−1) bond critical points (BCPs) have been localized. No BCP has been observed between Ru3 and Ru4, and two Ru-H BCPs have been found instead. The AIM analysis indicates that the hydride also forms a bond with the copper center, justifying its position with respect to the Ru_2Cu triangle. The lower strength of the Ru2-Ru3 and Ru2-Ru4 interactions compared to Ru1-Ru2, Ru1-Ru3 and Ru1-Ru4 is confirmed by the less negative values of electron density (ρ) and potential energy density (V) at BCP.

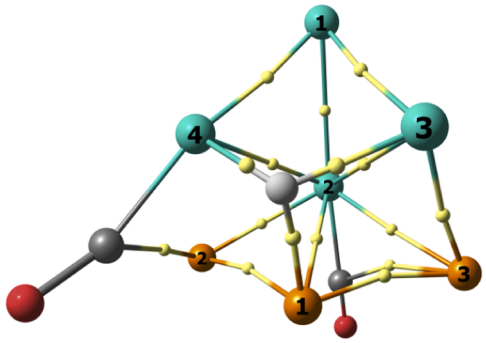

Fig. 4. DFT-optimized structure of **2** with Br atoms and selected CO ligands omitted for clarity (turquoise, Ru; orange, Cu; red O; grey C; white H). The BCPs summarized in Table 1 are represented with small yellow spheres.

The seven Ru-Cu contacts [2.6041(7)-2.7808(7) Å] are comparable to the Ru-Cu bonds reported for similar heterometallic carbonyl clusters [41–45,55–59]. Only four Ru-Cu BCPs have been however localized, as summarized in Table 1. Ru2 is involved in localized bonds with all the three copper centers with comparable ρ and V values. Cu3 presents an interaction of comparable strength also with Ru3, while a symmetric Cu2-Ru4 BCP is absent. The unexpected asymmetry between Cu3 and Cu2 can be justified by the different interactions of the copper centers with the carbonyl ligands. A Cu-C BCP has been in fact localized between Cu2 and the close Ru4-bonded carbonyl ligand, while a symmetric BCP involving Cu3 is absent. On the other hand, a BCP is present between Cu3 and a Ru2-bonded CO (Fig. 4), but the ρ and V values are meaningfully less negative compared to the other Ru-Cu BCPs. It is likely to be supposed that selected Cu-Ru interactions could be replaced by Cu-C ones and vice versa, and that a dynamic situation could exist in the real system.

This point is further supported by the SC-XRD structure, which shows that the three CO ligands pointing toward the three Cu fragments [CO6, CO9 and CO12, bonded to Ru2, Ru3 and Ru4, respectively] display short Cu···C(O) contacts [2.558(5)-2.657(5) Å]. The bridge asymmetry parameter (α) [60] of these CO ligands [α_{CO6} 0.337(6), α_{CO9} 0.352(14), α_{CO12} 0.388(6)] is within the range of semi-bridging CO ligands [α = 0.1–0.6], but the Ru2-C6-O6 [170.1(4)°], Ru3-C9-O9 [172.0(4)°], and Ru4-C12-O12 [171.7(5)°] angles display only minor deviations from linearity. It is noteworthy that in the above mentioned AIM analysis, BCPs were found only for CO6 and CO12. This suggests that the interactions between CO ligands and Cu centers are rather weak and may slightly change passing from the isolated anion to the solid state. Indeed, such short Cu···C(O) interactions are rather debated in the literature and usually considered as very weak. Disregarding the interactions with copper, all 12 CO ligands are terminally bonded, three per each Ru atom.

Two cuprophilic interactions are present, that is, Cu1-Cu2 [2.6380(8) Å] and Cu1-Cu3 [2.5809(8) Å]. Two comparable BCPs have been localized between the copper atoms in the DFT-optimized structure of **2**. According to Bianchi's classification [61], the Cu-Cu contacts can be considered metal-metal bonds because of the positive Laplacian of electron density ($\nabla^2\rho$) and negative energy density (E) at BCP, as occurs also for the Ru-Ru interactions. The M-C and M-H (3,−1) BCPs collected in Table 1 respect Bianchi's definition of dative bonds.

The formal oxidation state of the Cu atoms in **2** is +1, but charge decomposition analysis (CDA) [62] calculations indicate a noticeable electron transfer from the ruthenium carbonyl cluster to the CuBr fragments, from 0.34 to 0.40 electrons. Accordingly, the Hirshfeld partial charges on the Cu atoms in **2** are in the 0.107 - 0.143 a.u. range, much lower than the value calculated for free CuBr (0.362 a.u.) [63]. The previously described Cu-Cu bonds can be a consequence of the electron-rich nature of the Cu centers.

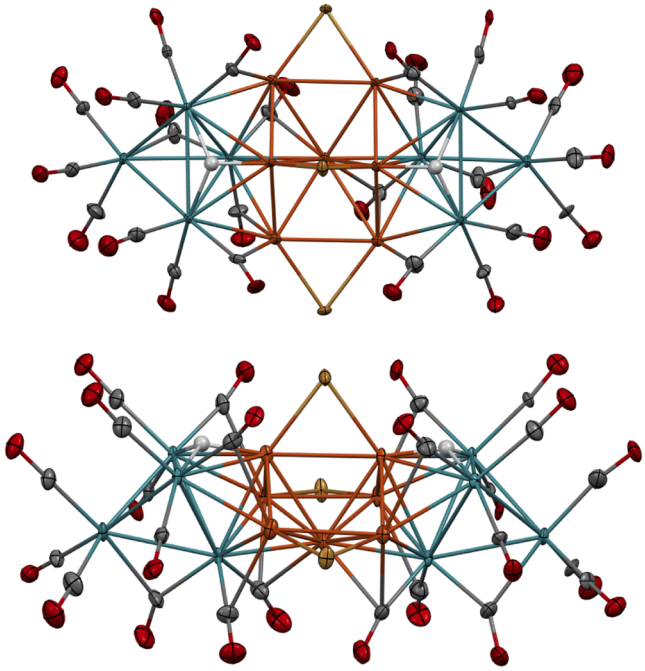

Fig. 5. Two views of the molecular structure of **3** (turquoise, Ru; orange, Cu; brown, Br; red O; grey C; white H).

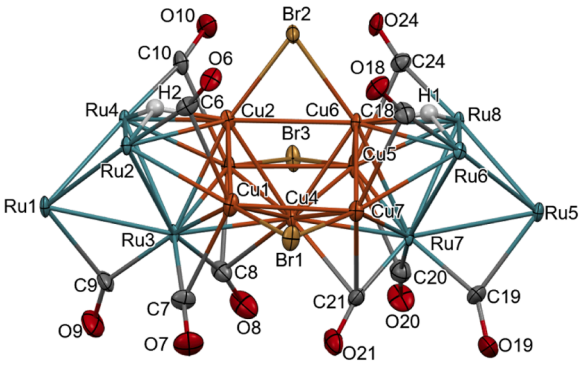

Fig. 6. Labelling scheme of **3** (turquoise, Ru; orange, Cu; brown, Br; red O; grey C; white H). Terminal CO ligands are not represented for clarity.

2.2.2. $[H_2Ru_8(CO)_{24}Cu_7Br_3]^{2-}$ (3)

The SC-XRD structure of **3** (Figs. 5 and 6; Table S2 in the Supporting Information) is very similar to that previously reported for the analogous chloride derivative $[H_2Ru_8(CO)_{24}Cu_7Cl_3]^{2-}$ [41]. Dianion **3** may be formally obtained from the condensation of two **2** clusters and one Cu^+ ion with the elimination of three bromides. The structure of the HRu_4Cu_3 core of **2** is retained within the two moieties of **3**, comprised the location of the hydride ligands, and all the bonding parameters are very similar. The μ_3 coordination mode of the hydrides has been confirmed by both molecular and periodic DFT calculations.

Alternatively, **3** may be described as composed of two tetrahedral cluster trianions of type **1** sandwiching a $[Cu_7Br_3]^{4+}$ copper cluster core.

Table 2
Computed Hirshfeld charges of the Cu centers in 3 and in a hypothetical free $[Cu_7Br_3]^{4+}$ unit.

	3	$[Cu_7Br_3]^{4+}$
Cu4	0.078	0.278
Cu1, Cu3, Cu5, Cu7	0.130 - 0.135	0.506 - 0.510
Cu2, Cu6	0.106	0.413

As in the case of **2**, the hydrides migrate from the Ru_3 face of **1** to Ru_2Cu faces of **3**, further confirming some affinity to Cu of the hydride ligands.

The Cu_7 cluster core may be described as two fused square-based pyramids that share a common triangular face. Three bromide ligands each symmetrically bridge two of the atoms in the core. Only Cu4 is not involved in the Br-bridges, and it displays a high metal connectivity, being bonded to six Cu and two Ru atoms. Cu2 and Cu6 have seven metal-metal contacts (four Cu-Cu and three Cu-Ru), whereas Cu1, Cu3, Cu5 and Cu7 show a metal connectivity of five (three Cu-Cu and two Cu-Ru). Overall, the Cu_7 core displays 13 Cu-Cu bonding contacts, which are rather spread [2.551(3)-2.786(3) Å], with the three Br-bridged Cu-Cu edges [2.721(4)-2.786(3) Å] significantly longer than the other ten edges [2.551(3)-2.646(4) Å]. The high Cu-Cu connectivity may be ascribed to some electron donation from the two $[HRu_4(CO)_{12}]^{3-}$ clusters to the $[Cu_7Br_3]^{4+}$ copper cluster core, which somehow increases the electron density on Cu and favors metal bonding. The result of CDA calculations on the DFT-optimized structure of **3** is the net donation of 1.03 electrons from each $[HRu_4(CO)_{12}]^{3-}$ fragment to the central $[Cu_7Br_3]^{4+}$ core. Such a charge transfer is evident on comparing the Hirshfeld charges of the Cu centers in **3** and in a hypothetical free $[Cu_7Br_3]^{4+}$ unit, as reported in Table 2.

The CO stereochemistry of **3** is different from that of **2**. Disregarding for the moment Cu···C(O) contacts, each Ru_4 unit of **3** contains one Ru-Ru edge-bridging and 11 terminal CO ligands, whereas only terminal carbonyls were present in **2**. This is likely to be due to the steric requirements to accommodate the larger $[Cu_7Br_3]^{4+}$ moiety, compared to the three CuBr fragments of **2**. Indeed, the μ-CO ligand within each Ru_4 unit of **3** formally originates from a CO ligand of **2** which points toward the additional Cu ion during the formal condensation of two type **2** clusters and Cu^+ to yield **3** (Fig. 7). The asymmetry parameters for these Ru-Ru μ-CO ligands [α_{CO9} 0.16(2), α_{CO19} 0.14(2)] are very close to the values expected for symmetrical edge bridging carbonyls [$\alpha < 0.1$], as also confirmed by the Ru3-C9-O9 [145(2) °] and Ru5-C19-O19 [130.5 (18) °] angles. In addition, some Cu···C(O) contacts [2.35(2)-2.54 (2)Å] are present.

The AIM analysis on the DFT-optimized structure of **3** (Table 3) has

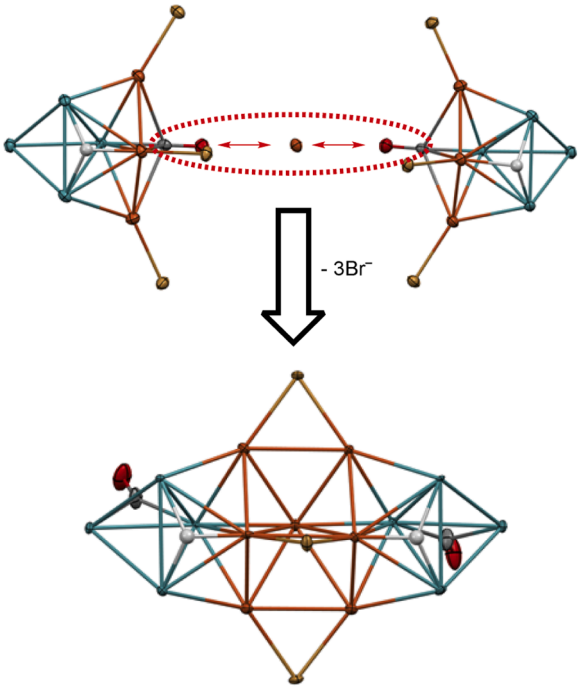

Fig. 7. Formal condensation of two $[HRu_4(CO)_{12}(CuBr)_3]^{3-}$ (**2**) clusters and one Cu^+ ion to give **3**. The steric repulsion between one CO ligand per cluster **2** unit and the additional Cu^+, which causes the CO rearrangement, is evidenced.

Table 3
Selected average properties at Ru-Ru, Ru-H, Ru-Cu, Cu-H, Cu-C and Cu-Cu BCPs for 3.

Attractors	ρ (a.u.)	V (a.u.)	E (a.u.)	$\nabla^2\rho$ (a.u.)
Ru1-Ru2 / Ru5-Ru8	0.0433	−0.0312	−0.0105	0.0405
Ru1-Ru4 / Ru5-Ru6	0.0466	−0.0335	−0.0120	0.0379
Ru3-Ru4 / Ru6-Ru7	0.0416	−0.0297	−0.0095	0.0430
Ru2-Ru3 / Ru7-Ru8	0.0408	−0.0289	−0.0092	0.0418
Ru2-H2 / Ru8-H1	0.0733	−0.0826	−0.0211	0.1618
Ru4-H2 / Ru6-H1	0.0755	−0.0858	−0.0223	0.1643
Cu2-H2 / Cu6-H1	0.0456	−0.0420	−0.0068	0.1139
Ru4-Cu2 / Ru6-Cu6	0.0391	−0.0324	−0.0069	0.0740
Ru2-Cu2 / Ru8-Cu6	0.0387	−0.0319	−0.0069	0.0728
Ru4-Cu3 / Ru6-Cu7	0.0455	−0.0384	−0.0098	0.0748
Ru3-Cu4 / Ru7-Cu4	0.0486	−0.0418	−0.0105	0.0834
Ru3-Cu2 / Ru7-Cu6	0.0378	−0.0284	−0.0068	0.0591
Ru3-Cu3 / Ru7-Cu7	0.0425	−0.0352	−0.0084	0.0736
Cu1-C6 / Cu5-C24	0.0522	−0.0481	−0.0074	0.1333
Cu4-C8 / Cu4-C21	0.0551	−0.0531	−0.0088	0.1416
Cu3-C8 / Cu7-C21	0.0421	−0.0350	−0.0039	0.1084
Cu1-Cu4 / Cu4-Cu5	0.0367	−0.0281	−0.0059	0.0648
Cu2-Cu4 / Cu4-Cu6	0.0384	−0.0311	−0.0057	0.0785
Cu3-Cu4 / Cu4-Cu7	0.0359	−0.0289	−0.0055	0.0717
Cu2-Cu3 / Cu6-Cu7	0.0381	−0.0303	−0.0061	0.0724
Cu1-Cu2 / Cu5-Cu6	0.0390	−0.0316	−0.0063	0.0762

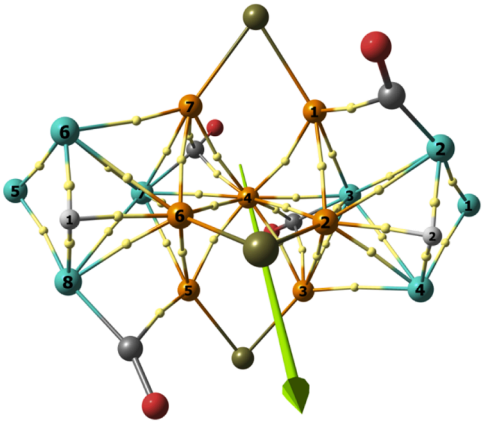

Fig. 8. DFT-optimized structure of **3** with selected CO ligands omitted for clarity (turquoise, Ru; orange, Cu; red O; brown, Br; grey C; white H). The BCPs summarized in Table 3 are represented with small yellow spheres. The C_2 symmetry axis is green colored.

revealed approximate C_2 symmetry of the electronic structure. The symmetry axis is shown in Fig. 8. Four Ru-Ru BCPs are present for each half of the compound, since no Ru-Ru BCP has been localized between the Ru centers bridged by hydride or carbonyl ligands. As in **2**, three M-H BCPs are present around the hydrides of **3**. The comparison of the AIM data in Tables 1 and 3 indicates that Cu-H bonds are weaker in **3** with respects to **2**, while the Ru-H interactions have similar strength. Each $HRu_4(CO)_{12}$ unit is connected to the central Cu_7Br_3 core by means of six Ru-Cu BCPs. The most negative ρ and V values correspond to the BCP between the central Cu4 and the Ru3 centers (and for the symmetry-related Cu4-Ru7 interaction). Seven Cu-Ru contacts are present in the SC-XRD structure for each halve of the molecule, but no BCP has been found between Cu1 and Ru2 (and between Cu5 and Ru8) in the DFT-optimized structure, probably because of the Cu1-C6 and Cu5-C24 bonds formed by the copper centers with the close carbonyl ligands. Further Cu-C BCPs involve the Ru3-bonded carbonyl ligand close to the Cu3 and Cu4 atoms (and the Ru7-bonded carbonyl close to Cu4 and Cu7). The E and $\nabla^2\rho$values allow to consider all the Cu-C interactions as dative bonds.

Ten Cu-Cu BCPs have been localized in the DFT-optimized structure of **3** with comparable ρ and V values, and with E and $\nabla^2\rho$ values in line with metal-metal bonds (Table 3). Considering the thirteen Cu-Cu short contacts present in the structure, Cu-Cu localized bonds are absent between the copper centers connected by μ-Br ligands (Fig. 8).

2.2.3. $[HRu_8(CO)_{24}Cu_6Br_2]^{3-}$ (4)

The molecular structure of **4** may be described as composed of one $[HRu_4(CO)_{12}]^{3-}$ (**1**) and one $[Ru_4(CO)_{12}]^{4-}$ (**1-H**$^+$) cluster sandwiching a $[Cu_6Br_2]^{4+}$ core (Figs. 9 and 10; Table S3 in the Supporting Information). Considering such a partitioning scheme, CDA calculations on the DFT-optimized structure of **4** revealed a noticeable electron transfer from the Ru_4 fragments to the $[Cu_6Br_2]^{4+}$ core, in line with the results previously described for **3**. As expected, the net donation is higher from the more negative $[Ru_4(CO)_{12}]^{4-}$ fragment (1.303 electrons) respect to $[HRu_4(CO)_{12}]^{3-}$ (0.808 electrons). The average Hirshfeld charge of the Cu atoms in **4** is 0.115 a.u., much lower than the value obtained for $[Cu_6Br_2]^{4+}$ (0.547 a.u.). Alternatively, **4** may be viewed as the result of the condensation of one $[HRu_4(CO)_{12}Cu_3]$ and one $[Ru_4(CO)_{12}Cu_3]^-$ unit with the addition of two Cu-Cu bridging Br^- ligands (Fig. 11).

The structure of the $[HRu_4(CO)_{12}Cu_3]$ unit is very similar to that

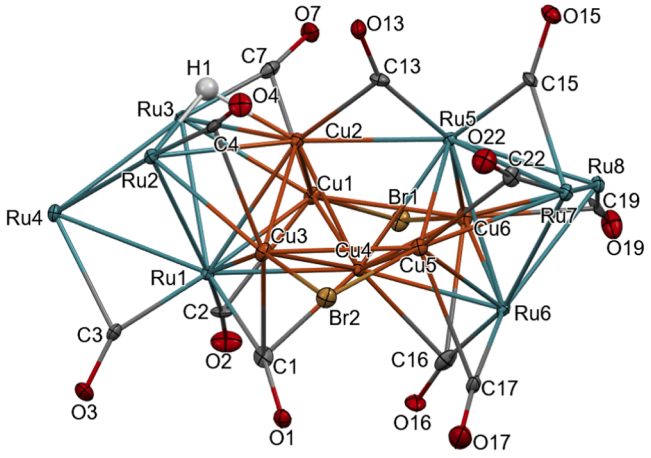

Fig. 10. Labelling scheme of **4** (turquoise, Ru; orange, Cu; brown, Br; red O; grey C; white H). Terminal CO ligands are not represented for clarity.

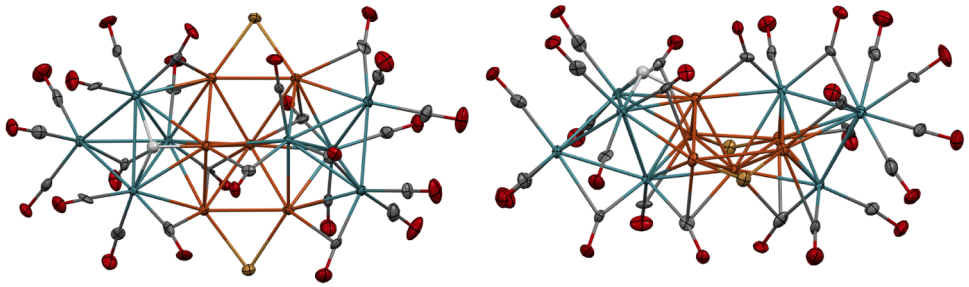

Fig. 9. Two views of the molecular structure of **4** (turquoise, Ru; orange, Cu; brown, Br; red O; grey C; white H).

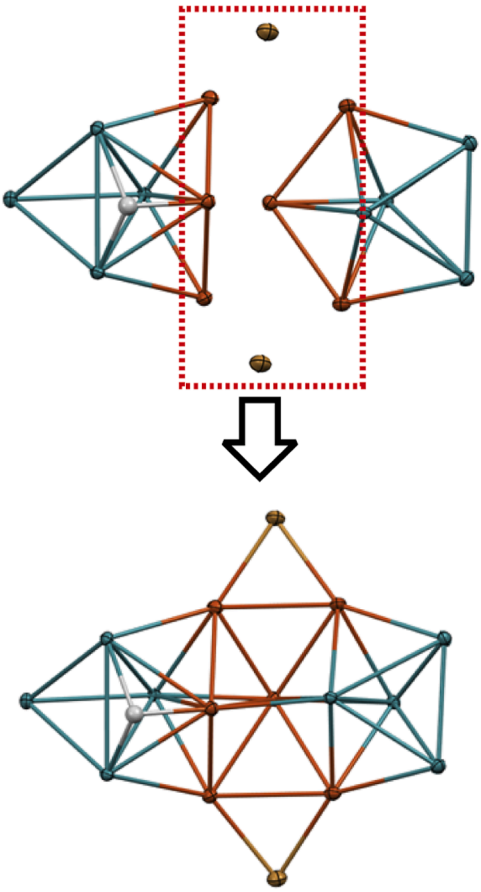

Fig. 11. Formal condensation of one $[HRu_4(CO)_{12}Cu_3]$ and one $[Ru_4(CO)_{12}Cu_3]^-$ unit with the addition of two Br^- ligands to yield **4**.

found in **3**. Thus, one Cu atom is capping a Ru_3 face of the Ru_4 tetrahedron, and the two further Cu atoms are capping two Ru_2Cu faces of the resulting Ru_4Cu trigonal bipyramid. The unique hydride is located on the third Ru_2Cu face and, disregarding the Cu···C(O) interactions, 11 carbonyls are terminally bonded to the Ru_4 tetrahedron and one is bridging a Ru-Ru edge [α_{CO3} 0.209(11), Ru1-C3-O3 149.5(8)°]. As for **3**, the position of the hydride has been confirmed by periodic DFT calculations on the cesium salt of **4**. After full optimization of the geometry of **4** with the r^{2}SCAN method, four Ru-Ru, two Ru-H and one Cu-H BCPs have been localized in the $HRu_4(CO)_{12}Cu_3$ fragment, roughly comparable to those previously described for **3** (Table 4 and Fig. 12). On the other hand, the number of Ru-Cu BCPs in this unit is four, less than the six Ru-Cu BCPs present in each half of **3**. The Cu atom capping the Ru_3 triangle is involved in three Ru-Cu metal-metal bonds in 3 and in only one in the $HRu_4(CO)_{12}Cu_3$ fragment of 4. Such a difference is possibly related to the presence in 4 of a strong Cu-C interaction (see the BCP between Cu2 and C13), absent in compound 3.

A different coordination of the Cu atoms is observed in the $[Ru_4(CO)_{12}Cu_3]^-$ unit. Indeed, Cu4 bridges the Ru5-Ru6 edge, whereas Cu5 and Cu6 are capping the Ru5Ru6Ru8 and Ru5Ru6Ru7 faces, respectively. A similar metal arrangement has been previously found in a second isomer of $[HRu_4(CO)_{12}(AuPPh_3)_3]$ [49], $[Ru_3Ir(CO)_{12}(AuPPh_3)_3]$ [21], and $[HFe_4(CO)_{12}(AuPPh_3)_3]$, [64]. Not considering for the moment the weak Cu···C(O) interactions, the Ru_4 tetrahedron displays 12 CO ligands, 11 terminally bonded and one bridging a Ru-Ru edge [α_{CO15} 0.113(10), Ru5-C15-O15 141.1(8)]. Five Ru-Ru BCPs are present in the $Ru_4(CO)_{12}Cu_3$ unit of the DFT-optimized structure, one more compared to the $HRu_4(CO)_{12}Cu_3$ fragment probably because of the lack of the bridging hydride. Seven Ru-Cu BCPs have been localized in $Ru_4(CO)_{12}Cu_3$, since a Ru-Cu BCP is present between each

Table 4
Selected properties at Ru-Ru, Ru-Cu, Ru-H, Cu-H, Cu-Cu and Cu-C BCPs for 4.

Attractors	ρ (a.u.)	V (a.u.)	E (a.u.)	$\nabla^2\rho$(a.u.)
Ru1-Ru2	0.0405	−0.0288	−0.0090	0.0430
Ru1-Ru3	0.0406	−0.0293	−0.0091	0.0444
Ru2-Ru4	0.0452	−0.0318	−0.0114	0.0358
Ru3-Ru4	0.0412	−0.0288	−0.0097	0.0380
Ru5-Ru6	0.0311	−0.0199	−0.0049	0.0409
Ru5-Ru7	0.0427	−0.0308	−0.0103	0.0412
Ru6-Ru7	0.0445	−0.0324	−0.0108	0.0428
Ru6-Ru8	0.0381	−0.0276	−0.0080	0.0464
Ru7-Ru8	0.0451	−0.0338	−0.0113	0.0443
Ru2-H1	0.0729	−0.0820	−0.0209	0.1613
Ru3-H1	0.0717	−0.0890	−0.0201	0.1628
Cu2-H1	0.0517	−0.0516	−0.0104	0.1231
Ru1-Cu1	0.0397	−0.0318	−0.0075	0.0675
Ru1-Cu2	0.0341	−0.0248	−0.0057	0.0537
Ru1-Cu3	0.0412	−0.0337	−0.0079	0.0712
Ru2-Cu3	0.0459	−0.0388	−0.0100	0.0753
Ru5-Cu4	0.0355	−0.0271	−0.0061	0.0596
Ru5-Cu5	0.0407	−0.0321	−0.0081	0.0633
Ru5-Cu6	0.0437	−0.0395	−0.0085	0.0900
Ru6-Cu4	0.0452	−0.0399	−0.0088	0.0889
Ru6-Cu5	0.0408	−0.0327	−0.0080	0.0665
Ru7-Cu6	0.0425	−0.0361	−0.0083	0.0778
Ru8-Cu5	0.0425	−0.0335	−0.0090	0.0618
Cu2-C13	0.0780	−0.0915	−0.0228	0.1834
Cu3-C1	0.0428	−0.0360	−0.0041	0.1109
Cu4-C1	0.0593	−0.0596	−0.0111	0.1498
Cu4-C16	0.0511	−0.0469	−0.0071	0.1309
Cu6-C16	0.0513	−0.0466	−0.0070	0.1303
Cu6-C19	0.0482	−0.0432	−0.0059	0.1251
Cu1-Cu2	0.0397	−0.0333	−0.0061	0.0840
Cu1-Cu4	0.0377	−0.0304	−0.0057	0.0760
Cu1-Cu7	0.0599	−0.0586	−0.0111	0.1456
Cu2-Cu3	0.0381	−0.0310	−0.0058	0.0775
Cu2-Cu4	0.0425	−0.0385	−0.0064	0.1031
Cu3-Cu4	0.0362	−0.0297	−0.0054	0.0756
Cu4-Cu5	0.0369	−0.0284	−0.0060	0.0654
Cu4-Cu6	0.0345	−0.0257	−0.0059	0.0555

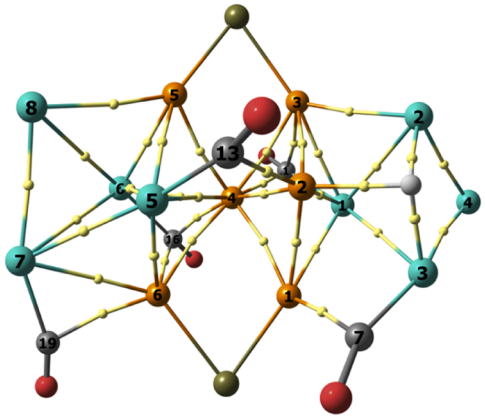

Fig. 12. DFT-optimized structure of **4** with selected CO ligands omitted for clarity (turquoise, Ru; orange, Cu; brown, Br; red O; grey C; white H). The BCPs summarized in Table 4 are represented with small yellow spheres.

Cu atom and the close Ru centers.

As observed for the other Ru-Cu heterometallic carbonyl clusters, the Ru-Ru bonding distances not spanned by Cu atoms [2.8075(11)-2.8519 (11) Å] are shorter than the others [2.7983(11)-3.0584(11) Å]. Ru5-Ru8 [2.7983(11) Å] is apparently an exception, but this is likely to be because this edge is bridged both by Cu5 and a μ-CO ligand, which have opposite influences on the Ru-Ru distance. Ru5-Ru8 is also the only Ru-Ru edge of the $[Ru_4(CO)_{12}]$ tetrahedron for which a BCP has not been localized. The 17 Ru-Cu bonds [2.5947(14)-2.8642(14) Å] are rather spread, as found also in **2** [2.6041(7)-2.7808(7) Å] and **3** [2.584(3)-

2.793(3) Å].

The $[Cu_6Br_2]^{4+}$ core displays 9 Cu-Cu contacts [2.4669(16)-2.7095(17) Å], the longest ones being those bridged by the two Br-ligands [Cu1-Cu6 2.6596(17) Å, Cu3-Cu5 2.7095(17) Å]. Seven Cu-Cu BCPs are present in the DFT-optimized structure, since no BCP was found for the Cu centers bridged by μ-Br, in line with what was observed in compound **3**. Some weak Cu···C(O) contacts are present [2.145(10)-2.619(10) Å], with α in the range 0.183(12)-0.373(12) and Ru-C-O angles which in some cases sensibly deviate from linearity [157.7(8)-173.8(9)°]. As summarized in Table 4, the AIM analysis suggests the presence of Cu-C dative bonds for five carbonyl ligands of the compound, two of them interacting with two different Cu atoms. The previously mentioned BCP between Cu2 and C13 is characterized by particularly negative ρ and V values compared to the other Cu-C BCPs, according to the short Cu-C distance obtained from gas-phase calculations, 2.081 Å, slightly shorter than the experimental value [2.145(10) Å]. Even if the number of Cu-C BCPs is always lower than the contacts observed in the X-ray structures, gas-phase DFT calculations on **2**–**4** support the idea that the structures of the clusters could be almost in part stabilized by electron-sharing interactions between electron-rich copper centers and carbonyl ligands.

2.2.4. $[Ru_5(CO)_{15}(CuMeCN)_2]$ (5)

The molecular structure of **5** may be described as composed of a trigonal bipyramidal $[Ru_5(CO)_{15}]^{2-}$ cluster capped on two adjacent triangular faces, sharing the same equatorial-equatorial Ru3-Ru4 edge, by two $[CuMeCN]^+$ fragments (Fig. 13 and Table S4 in the Supporting Information). A similar Ru_5M_2 cluster core was previously observed only in the case of $[Ru_5(CO)_{15}Au_2(dppm)]$, [65], and in the Os congener $[Os_5(CO)_{15}Au_2(dppm)]$, [66]. The structures of the homoleptic carbonyl dianions $[M_5(CO)_{15}]^{2-}$ (M = Fe, Ru, Os) have not been reported. A trigonal bipyramidal structure has been found in related group 8 homometallic carbonyl clusters such as $[HFe_5(CO)_{14}]^{3-}$ [67], $HOs_5(CO)_{15}]^-$ [68], $Os_5(CO)_{15}I]^-$ [69], $[Os_5(CO)_{16}]$ [70], $[H_2Os_5(CO)_{14}(Py)]$ [71], and $[Os_5(CO)_{15}(CNBu^t)]$ [72]. An Os_5 trigonal bipyramidal cage was found also in $[Os_5(CO)_{15}(AuPPh_3)_2]$ [22], but the two $AuPPh_3$ fragments are capping two triangular Os_3 faces sharing a common apical-equatorial Os-Os edge. The structure of $[H_2Ru_6(CO)_{17}]$ [73] is also of some relevance to this work, since it contains a $Ru_5(CO)_{14}$ trigonal bipyramidal structure, with three adjacent triangular faces sharing the same apical Ru atom capped by the two hydrides and a $Ru(CO)_3$ fragment.

CDA calculations on the DFT-optimized structure of **5** indicate that 0.759 electrons are globally drained from $[Ru_5(CO)_{15}]^{2-}$ by the $[CuMeCN]^+$ units. Despite this result, the comparison of the DFT-optimized structure of $[Ru_5(CO)_{15}]^{2-}$ with the same fragment present in **5** reveals that the trigonal pyramidal arrangement of the Ru centers and the coordination modes of the carbonyl ligands are comparable, the root mean square deviation (RMSD) being equal to 0.496 Å (Fig. 14).

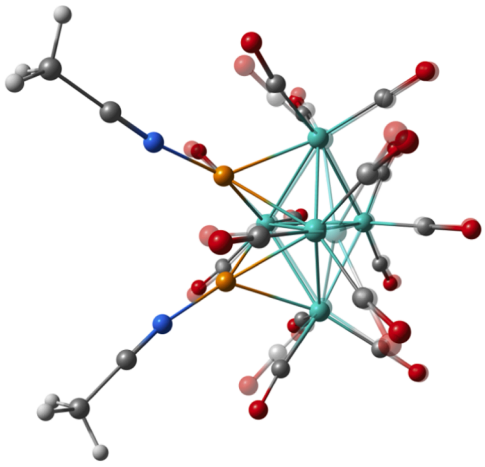

Fig. 14. DFT-optimized structure of **5** (turquoise, Ru; orange, Cu; red O; grey C) superimposed to the DFT-optimized structure of $[Ru_5(CO)_{15}]^{2-}$ (semi-transparent tones).

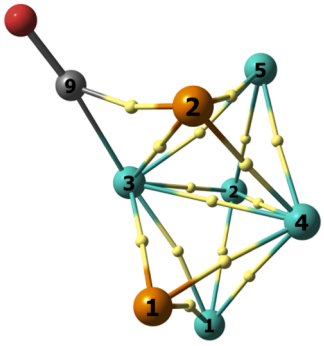

Fig. 15. DFT-optimized structure of **5** with CH_3CN and selected CO ligands omitted for clarity (turquoise, Ru; orange, Cu; red O; grey C). The BCPs summarized in Table 5 are represented with small yellow spheres.

5 possesses 72 cluster valence electrons (CVE), in agreement with the Effective Atomic Number rule (EAN) for a trigonal bipyramid [74].

The nine Ru-Ru [2.6894(12)-2.9839(12) Å] and six Ru-Cu [2.5655(16)-2.7358(16) Å] contacts are essentially single bonds, comparable to those found in the other clusters herein discussed. The AIM analysis on the DFT-optimized structure indicates the presence of nine Ru-Ru and

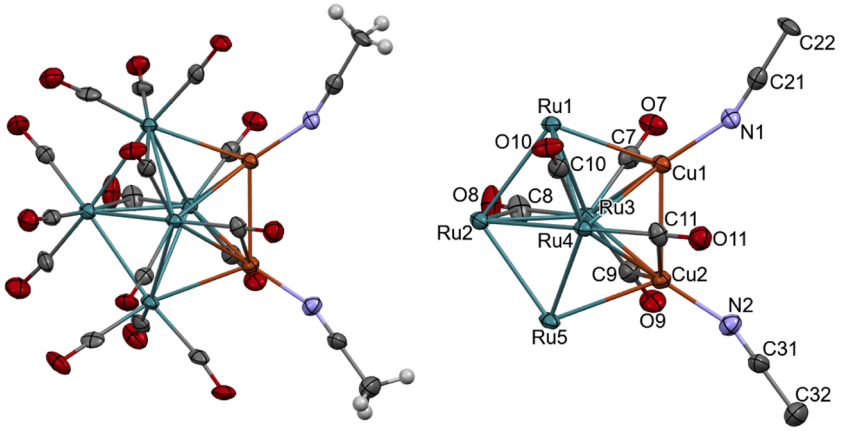

Fig. 13. Molecular structure and labelling scheme of **5** (turquoise, Ru; orange, Cu; brown, Br; blue, N; red O; grey C; white H).

Table 5
Selected properties at Ru-Ru, Ru-Cu and Cu-C BCPs for 5.

Attractors	ρ (a.u.)	V (a.u.)	E (a.u.)	$\nabla^2\rho$ (a.u.)
Ru1-Ru2	0.0440	−0.0312	−0.0110	0.0369
Ru1-Ru3	0.0381	−0.0252	−0.0082	0.0354
Ru1-Ru4	0.0520	−0.0469	−0.0132	0.0820
Ru2-Ru3	0.0478	−0.0402	−0.0118	0.0662
Ru2-Ru4	0.0440	−0.0316	−0.0107	0.0406
Ru2-Ru5	0.0459	−0.0336	−0.0117	0.0408
Ru3-Ru4	0.0408	−0.0317	−0.0088	0.0569
Ru3-Ru5	0.0393	−0.0262	−0.0087	0.0350
Ru4-Ru5	0.0520	−0.0458	−0.0134	0.0762
Ru1-Cu1	0.0395	−0.0287	−0.0082	0.0493
Ru3-Cu1	0.0505	−0.0473	−0.0112	0.0993
Ru4-Cu1	0.0418	−0.0333	−0.0086	0.0644
Ru3-Cu2	0.0494	−0.0460	−0.0107	0.0981
Ru4-Cu2	0.0421	−0.0347	−0.0085	0.0706
Ru5-Cu2	0.0403	−0.0306	−0.0083	0.0564
Cu2-C9	0.0479	−0.0420	−0.0058	0.1214

six Ru-Cu BCPs (Fig. 15 and Table 5). The molecule is roughly symmetric with respect to the equatorial plane containing Ru2, Ru3 and Ru4, thus the Ru-Ru and Ru-Cu BCPs related by this symmetry element have similar properties. The equatorial Ru3 and Ru4 centers are not symmetric and are involved in different metal-metal interactions. For instance, the Ru-Ru bonds between Ru4 and the apical Ru atoms are the strongest, while those between Ru3 and the apical centers are the weakest. As another example, Ru3 forms stronger bonds with the Cu centers compared to Ru4.

A cuprophilic interaction is present between the two Cu atoms [Cu1-Cu2 2.6726(18) Å], but no Cu-Cu BCP has been localized in the DFT-optimized structure (computed Cu-Cu distance 2.670 Å), even if the average Hirshfeld partial charge of the Cu centers (0.174 a.u.) is comparable with the values computed for the other clusters. Moreover, no ring critical point was localized in the $RuCu_2$ triangles and no cage critical point in the Ru_2Cu_2 tetrahedron. Considering for the moment only the Ru atoms, among the 15 CO ligands, 13 are terminally bonded and two are semi-bridging on Ru-Ru edges [α_{CO8} 0.320(15), α_{CO10} 0.241 (13), Ru3-C8-O8 159.4(10)°, Ru4-C10-O10 156.2(10)°]. In addition, among the 13 carbonyls terminally bonded to Ru atoms, three of them display some weak Cu···C(O) contact [C7-Cu1 2.497(11) Å, C9-Cu2 2.404(13) Å, C11-Cu2 2.610(13) Å; α_{CO7} 0.324(14), α_{CO9} 0.269(16), α_{CO11} 0.373(16); Ru3-C7-O7 171.9(10)°; Ru3-C9-O9 170.5(11)°, Ru4-C11-O11 174.2(10)°]. Only one Cu-C BCP has been, however, found in the DFT-optimized structure of **5**, between Cu2 and C9.

3. Conclusions

Four new heterometallic Ru-Cu carbonyl clusters **2**–**5** have been synthesized and structurally characterized by SC-XRD. They can be viewed as composed of $[HRu_4(CO)_{12}]^{3-}$, $[Ru_4(CO)_{12}]^{4-}$ and $[Ru_5(CO)_{15}]^{2-}$ cluster anions interacting with CuBr, $[Cu(MeCN)]^+$, $[Cu_7Br_3]^{4+}$ and $[Cu_6Br_2]^{4+}$ frameworks. CDA analyses based on DFT calculations indicate a noticeable $Ru_x \rightarrow Cu_y$ charge transfer from the Ru cluster anions to the Cu(I)-based fragments. This reduces the formal oxidation state of copper considerably below +1, favoring direct Cu···Cu bonding. Indeed, all clusters **2**–**5** contain cuprophilic interactions with Cu···Cu contacts in the range 2.4669(16)-2.786(3) Å, comparable to other coprophilic interactions documented in the literature [2,4–6,11,14–17]. These are well below the sum of the van der Waals radii of two Cu atoms (2.80 Å) [15,75], and quite close to the average Cu-Cu bonding contact in metallic *ccp* Cu metal (2.556 Å) [76]. The presence of close Cu···Cu interactions in **2**–**5** is further corroborated by the presence of BCPs as computed by DFT studies.

The present findings lend further support to the idea that heterometallic carbonyl clusters are suitable platforms for testing weak intramolecular metallophilic interactions [2,20–28,77–80]. From the other side, the interaction with metal-based fragments may be used to stabilize otherwise elusive or unstable metal carbonyl cluster anions, such as $[Ru_4(CO)_{12}]^{4-}$ and $[Ru_5(CO)_{15}]^{2-}$. Indeed, only $[HRu_4(CO)_{12}]^{3-}$ has been isolated and fully characterized as a free species [81].

4. Experimental

4.1. General procedures

All reactions and sample manipulations were carried out using standard Schlenk techniques under nitrogen and in dried solvents. All the reagents were commercial products (Aldrich) of the highest purity available and used as received, except $[NEt_4]_3[HRu_4(CO)_{12}]$, which has been prepared according to the literature [81]. Analyses of C, H and N were obtained with a Thermo Quest Flash EA 1112NC instrument. IR spectra were recorded on a Perkin Elmer Spectrum One interferometer in CaF_2 cells. ^1H NMR measurements were performed on a Varian Mercury Plus 400 MHz and Bruker Ascend Avance Neo 600 MHz spectrometers. Chemical shifts were referenced to the residual protonated fraction of the solvent. Molecular structures were visualized and illustrated using Mercury software [82].

4.2. Synthesis of $[NEt_4]_3$ $[HRu_4(CO)_{12}(CuBr)_3]$ (2) and $[NEt_4]_2$ $[H_2Ru_8(CO)_{24}Cu_7Br_3]\cdot 3CH_3COCH_3$ ($3\cdot 3CH_3COCH_3$)

$$[NEt_4]_3[HRu_4(CO)_{12}]$$
$$+ [Cu(MeCN)_4][BF_4] \xrightarrow[\text{r.t.,2h}]{\text{MeCN}\ [NEt_4]Br} [NEt_4]_3[HRu_4(CO)_{12}(CuBr)_3]$$
$$+ [NEt_4]_2[H_2Ru_8(CO)_{24}(Cu_7Br_3)]$$

Solid $[Cu(MeCN)_4][BF_4]$ (3 eq., 0.250 g, 0.795 mmol) was added in small portions to a solution of **1** (0.300 g, 0.265 mmol) and $[NEt_4]Br$ (0.167 g, 0.795 mmol) in CH_3CN (10 mL). The mixture was stirred at room temperature for 2 h, and then the solvent was removed in vacuum. The residue was washed with water (2 × 20 mL) and toluene (2 × 10 mL), dried under reduced pressure, and extracted with CH_2Cl_2 (10 mL). Then, the residue was extracted in acetone and layered with *n*-hexane, affording crystals of **2** suitable for SC-XRD (44 %). The CH_2Cl_2 solution was dried in vacuo and dissolved in acetone. Crystals of $\mathbf{3}\cdot 3CH_3COCH_3$ suitable for SC-XRD were obtained by layering *n*-hexane on acetone solution (40 %).

$[NEt_4]_3[HRu_4(CO)_{12}(CuBr)_3]$: $C_{36}H_{61}Br_3Cu_3N_3O_{12}Ru_4$ (1562.50): calcd. (%): C 27.67, H 3.93, N 2.69; found: C 27.89, H 3.78, N 2.95. IR (Acetone, 298 K) ν_{CO}: 2024(w), 1981(s) cm^{-1}. IR (MeCN, 298 K) ν_{CO}: 2037(w), 1985(s), 1929(w), 1773(m) cm^{-1}. IR (Nujol, 298 K) ν_{CO}: 2035 (w), 1982(s), 1958(m), 1923(m), 1880(w), 1859(w) cm^{-1}. ^1H NMR (Acetone-$d^6$298 K) δ: 3.48 (t, -CH_2-, 24H, NEt_4), 1.38 (q, -CH_3, 36H, NEt_4), −16.35 (s, 1H) ppm.

$[NEt_4]_2[H_2Ru_8(CO)_{24}Cu_7Br_3]\cdot 3CH_3COCH_3$: $C_{49}H_{58}Br_3Cu_7N_2O_{27}Ru_8$ (2600.04): calcd. (%): C 22.63, H 2.25, N 1.08; found: C 22.44, H 2.09, N 1.24. IR (CH_2Cl_2, 298 K) ν_{CO}: 2053(w), 2015(ms), 1986(s), 1944(m), 1721(mw) cm^{-1}. IR (Acetone, 298 K) ν_{CO}: 2051(w), 2022(ms), 1979(s), 1943(m) cm^{-1}. IR (Nujol, 298 K) ν_{CO}: 2052(w), 1977(s), 1931(m), 1784 (m) cm^{-1}. ^1H NMR (CD_2Cl_2, 298 K) δ: 3.37 (t, -CH_2-, 16H, NEt_4), 1.27 (q, -CH_3, 24H, NEt_4), −17.45 (s, 2H) ppm.

4.3. Synthesis of $[NEt_4]_3$ $[HRu_8(CO)_{24}Cu_6Br_2]\cdot CH_2Cl_2$ ($4\cdot CH_2Cl_2$)

$$[NEt_4]_3[HRu_4(CO)_{12}]$$
$$+ [Cu(MeCN)_4][BF_4] \xrightarrow[\text{r.t.,2h}]{\text{MeCN}\ [NEt_4]Br} [NEt_4]_2[H_2Ru_8(CO)_{24}(Cu_6Br_2)]$$

Solid $[Cu(MeCN)_4][BF_4]$ (1 eq., 0.0583 g, 0.186 mmol) was added to a solution of **1** (0.210 g, 0.186 mmol) and $[NEt_4]Br$ (0.117 g, 0.557 mmol) in MeCN (15 mL). The mixture was stirred at room temperature for 2 h, and then, the solvent was removed in vacuum. The residue was washed with water (2 × 20 mL) and toluene (2 × 10 mL), dried under reduced pressure, and extracted with CH_2Cl_2 (10 mL)*. Crystals of $[NEt_4]_3[HRu_8(CO)_{24}Cu_6Br_2]\cdot CH_2Cl_2$ (**4**·CH_2Cl_2) suitable for X-ray analyses were obtained by layering *n*-pentane on dichloromethane solution (57 %).

*The residue was extracted with acetone, and the product was identified as $[NEt_4]_2[H_2Ru_4(CO)_{12}]$ by FT-IR spectroscopy.

$[NEt_4]_3[HRu_8(CO)_{24}Cu_6Br_2]\cdot CH_2Cl_2$: $C_{49}H_{63}Br_2Cl_2Cu_6N_3O_{24}Ru_8$ (2498.54): calcd. (%): C 23.55, H 2.54, N 1.68; found: C 23.31, H 2.82, N 1.89. IR (CH_2Cl_2, 298 K) ν_{CO}: 2035(w), 1992(m), 1957(s), 1906(m), 1886(w), 1750(m) cm^{-1}. IR (acetone, 298 K) ν_{CO}: 2030(w), 1989(ms), 1955(s), 1905(m), 1888(m) cm^{-1}. IR (MeCN, 298 K) ν_{CO}: 2034(w), 1992 (ms), 1956(s), 1908(m), 1890(w), 1752(m) cm^{-1}. IR (Nujol, 298 K) ν_{CO}: 2017(m), 1985(s), 1960(vs), 1916(ms), 1750(m) cm^{-1}. ^1H NMR (CD_2Cl_2, 298 K) δ: 3.35 (t, -CH_2-, 24H, NEt_4), 1.26 (q, -CH_3, 36H, NEt_4), −19.19 (s, 1H) ppm.

4.4. Synthesis of $[Ru_5(CO)_{15}(CuMeCN)_2]\cdot CH_2Cl_2$ (5·CH_2Cl_2)

$$[NEt_4]_3[HRu_4(CO)_{12}] + [Cu(MeCN)_4][BF_4] \xrightarrow[r.t.,2h]{MeCN} [RU_5(CO)_{15}(CuMeCN)_2] + [RU_3(CO)_{12}]$$

Solid $[Cu(MeCN)_4][BF_4]$ (3.5 eq., 0.146 g, 0.464 mmol) was added in small portions to a solution of **1** (0.150 g, 0.132 mmol) in CH_3CN (15 mL). The mixture was stirred at room temperature for 2 h, and then the solvent was removed in vacuum. The residue was washed with water (2 × 20 mL) and toluene (2 × 10 mL), dried under reduced pressure, and extracted with CH_2Cl_2 (10 mL). Crystals of $[Ru_5(CO)_{15}(CuMeCN)_2]\cdot CH_2Cl_2$ (**5**·CH_2Cl_2) suitable for X-ray analyses were obtained by layering *n*-pentane on dichloromethane solution (26 %). The residue was then extracted in acetone, revealing a CO stretching frequency at higher wavenumber (2037 cm^{-1}) likely attributable to oxidized neutral by-product. A few crystals of $[Ru_3(CO)_{12}]$ (**7**) were also obtained.

$[Ru_5(CO)_{15}(CuMeCN)_2]\cdot CH_2Cl_2$: $C_{20}H_8Cl_2Cu_2N_2O_{15}Ru_5$ (1219.61): calcd. (%): C 19.70, H 0.66, N 2.30; found: C 19.32, H 0.95, N 2.02. IR (CH_2Cl_2, 298 K) ν_{CO}: 2054(w), 2028(vs), 2017(s), 1997(sh), 1948 (mw) cm^{-1}. IR (Nujol, 298 K) ν_{CO}: 2068(w), 2040(w), 2010(s), 1994(s), 1970 (ms), 1949(m) cm^{-1}. ^1H NMR (CD_2Cl_2, 298 K) δ: 2.86 (s, 6H, MeCN) ppm.

4.5. Synthesis of $[NEt_4]_2$ $[Ru_8(CO)_{26}Cu_2]$ (6)

$$[NEt_4]_3[HRu_4(CO)_{12}] + [Cu(MeCN)_4][BF_4] \xrightarrow[r.t.,2h]{\substack{MeCN \\ [NEt_4]Br}} [NEt_4]_2[Ru_8(CO)_{26}Cu_2]$$

Solid $[Cu(MeCN)_4][BF_4]$ (0.161 g, 0.512 mmol) was added in small portions to a solution of **1** (0.290 g, 0.256 mmol) and $[NEt_4]Br$ (0.0539 g, 0.256 mmol) in MeCN (15 mL). The mixture was stirred at room temperature for 2 h, and then the solvent was removed in vacuum. The residue was washed with water (2 × 20 mL) and toluene (2 × 10 mL), dried under reduced pressure, and extracted with CH_2Cl_2 (10 mL).* Crystals of $[NEt_4]_2[Ru_8(CO)_{26}Cu_2]$ (**6**) suitable for X-ray analyses were obtained by layering *n*-pentane on dichloromethane solution.

* The residue was extracted in acetone, and the product identified as a mixture of **2** and **3**.

$[NEt_4]_2[Ru_8(CO)_{26}Cu_2]$: IR ($CH_2Cl_2$, 298 K) ν_{CO}: 2042(w), 2005(sh), 1986(s), 1771(m) cm^{-1}. IR (acetone 298 K) ν_{CO}: 2039(w), 2000(sh), 1983(s) cm^{-1}.

4.6. X-ray crystallographic study

Crystal data and collection details for **2, 3**·$3CH_3COCH_3$, **4**·CH_2Cl_2, and **5**·CH_2Cl_2 are reported in Table S5 in the Supporting Information. The diffraction experiments were carried out on a Bruker APEX II diffractometer equipped with a PHOTON2 detector using Mo-Kα radiation. Data were corrected for Lorentz polarization and absorption effects (empirical absorption correction SADABS) [83]. Structures were solved by direct methods and refined by full-matrix least-squares based on all data using F^2 [84]. Hydrogen atoms were fixed at calculated positions and refined by a riding model, except hydride ligands which were tentatively located in the Fourier Difference Map and refined isotropically using the 1.2-fold *U* value of the parent metal atom. All non-hydrogen atoms were refined with anisotropic displacement parameters.

4.7. Computational details

Full geometry optimizations were carried out with the r^2-SCAN-3c method [51], based on the *meta*-GGA r^{2}SCAN functional and a triple-ζ Gaussian atomic orbital basis set, with corrections for London dispersion and basis set superposition error [85–87]. The stationary points were characterized as local minima by means of IR simulations, carried out using the harmonic approximation. Calculations were carried out using ORCA 5.0.3 and the output files were analyzed with Multiwfn, version 3.8 [88,89].

Periodic DFT calculations were carried out starting from the SC-XRD structures of **2, 3** and **4**. The lattice parameters and the atomic positions were taken from the .cif file and the ammonium cations were replaced with cesium. The geometry optimizations were limited to the positions of the hydride ligands. The PBEsol DFT functional [90] was used in combination with on-the-fly generated norm-conserving pseudopotentials [91]. The plane-wave basis set cut-off was set at 900 eV. The dispersion corrections from Tkatchenko and Scheffler were added [92]. Relativistic effects were accounted through the scalar Koelling-Harmon approximation [93]. The software used was CASTEP 20.1 [94].

CRediT authorship contribution statement

Cristiana Cesari: Writing – review & editing, Validation, Methodology, Investigation, Formal analysis, Data curation, Conceptualization. **Marco Bortoluzzi:** Writing – review & editing, Writing – original draft, Visualization, Methodology, Investigation, Formal analysis, Conceptualization. **Cristina Femoni:** Writing – review & editing, Validation, Data curation. **Francesca Forti:** Investigation, Formal analysis, Data curation. **Maria Carmela Iapalucci:** Validation, Methodology, Formal analysis. **Giorgia Scorzoni:** Investigation, Formal analysis, Data curation. **Stefano Zacchini:** Writing – review & editing, Writing – original draft, Validation, Funding acquisition, Conceptualization.

Declaration of competing interest

The authors declare that they have no known competing financial interests or personal relationships that could have appeared to influence the work reported in this paper.

Acknowledgments

We gratefully thank the University of Bologna for financial support.

Supplementary materials

Supplementary material associated with this article can be found, in the online version, at doi:10.1016/j.jorganchem.2025.123999.

Appendix A: Supplementary material

Supplementary Information as .pdf file.

DFT-optimized structures (.xyz and cif files).

CCDC 2500016 (**2**), 2500,017 (**3**·$3CH_3COCH_3$), 2500,018 (**4**·CH_2Cl_2), and 2500,019 (**5**·CH_2Cl_2) contain the supplementary crystallographic data for this paper. These data can be obtained free of charge from the Cambridge Crystallographic Data Centre.

Data availability

Data will be made available on request.

References

[1] P. Pyykkö, Strong closed-shell interactions in inorganic chemistry, Chem. Rev. 97 (1997) 597–636.

[2] S. Sculfort, P. Braunstein, Intramolecular d^{10}-d^{10} interactions in heterometallic clusters of the transition metals, Chem. Soc. Rev. 40 (2011) 2741–2760.

[3] H. Schmidbaur, A. Schier, Aurophilic interactions as a subject of current research: an up-date, Chem. Soc. Rev. 41 (2012) 370–412.

[4] M. Olaru, J.F. Kögel, R. Aoki, R. Sakamoto, H. Nishihara, E. Lork, S. Mebs, M. Vogt, J. Beckmann, Tri- and tetranuclear metal-string complexes with metallophilic d^{10}-d^{10} interactions, Chem. Eur. J. 26 (2020) 275–284.

[5] J. Zheng, Z. Lu, K. Wu, G.-H. Ning, D. Li, Coinage-metal-based cyclic trinuclear complexes with metal-metal interactions: theories to experiments and structures to functions, Chem. Rev. 120 (2020) 9675–9742.

[6] Q. Zheng, S. Borsley, G.S. Nichol, F. Duarte, S.L. Cockroft, The energetic significance of metallophilic interactions, Angew. Chem. Int. Ed. 58 (2019) 12617–12623.

[7] H. Schmidbaur, A. Schier, A briefing on aurophilicity, Chem. Soc. Rev. 37 (2008) 1931–1951.

[8] M.J. Katz, K. Sakai, D.B. Leznoff, The use of aurophilic and other metal-metal interactions as crystal engineering design elements to increase structural dimensionality, Chem. Soc. Rev. 37 (2008) 1884–1895.

[9] P. Pyykkö, Theoretical chemistry of gold. III, Chem. Soc. Rev. 37 (2008) 1967–1997.

[10] H. Schmidbaur, A. Schier, Argentophilic interactions, Angew. Chem. Int. Ed. 54 (2015) 746–784.

[11] N.V.S. Harisomayajula, S. Makovetskyi, Y.-C. Tsai, Cuprophilic interactions in and between molecular entities, Chem. Eur. J. 25 (2019) 8936–8954.

[12] H. Schmidbaur, A. Schier, Mercurophilic interactions, Organometallics 34 (2015) 2049–2066.

[13] J. Echeverría, J. Cirera, S. Alvarez, Mercurophilic interactions: a theoretical study on the importance of ligands, Phys. Chem. Chem. Phys. 19 (2017) 11645.

[14] Q. Wan, J. Yang, W.-P. To, C.-M. Che, Strong metal-metal Pauli repulsion leads to repulsive metallophilicity in closed shell d_8 and d_{10} organometallic complexes, Proc. Natl. Acad. Sci. U.S.A. 118 (2021) e2019265118.

[15] R. Bühler, R.M. Wolf, C. Gemel, J. Stephan, S.N. Deger, S. Kahlal, R.A. Fischer, J.-Y. Saillard, Cuprophilic interactions in polymeric $[Cu_{10}O_2(Mes)_6]_n$, Inorg. Chem. 63 (2024) 17617–17625.

[16] S. Wang, Z. Yang, X. Sun, M. Wu, K. Sheng, L. Zhang, B. Yang, K. Wang, Y. Sui, B. Zou, Anomalous pressure-induced blue-shifted emission of ionic copper-iodine clusters: the competitive effect between cuprophilic interactions and through-space interaction, Angew. Chem. Int. Ed. 64 (2025) e202414810.

[17] L. Zhang, X.-X. Li, Z.-L. Lang, Y. Liu, J. Liu, L. Yuan, W.-Y. Lu, Y.S. Xia, L.-Z. Dong, D.-Q. Yuan, Y.-Q. Lan, Enhanced cuprophilic interactions in crystalline catalysts facilitate the highly selective electroreduction of CO_2 to CH_4, J. Am. Chem. Soc. 143 (2021) 3808–3816.

[18] O. Hobza, J. Řezáč, Introduction: noncovalent interactions, Chem. Rev. 116 (2016) 4911–4912.

[19] R.M. Gomila, A. Frontera, The matere bond, Dalton Trans. 54 (2025) 3095–3105.

[20] C. Cesari, C. Femoni, F. Forti, M.C. Iapalucci, G. Scorzoni, S. Zacchini, Surface decorated metal carbonyl clusters: bridging organometallic molecular clusters and atomically precise ligated nanoclusters, Dalton Trans. 54 (2025) 2224–2251.

[21] R.D. Adams, P.J. Pellecchia, M.D. Smith, Q. Zhang, Iridium-ruthenium-gold cluster complexes: structures, and skeletal rearrangements, J. Organomet. Chem. 706-707 (2012) 20–25.

[22] R.D. Adams, Z. Luo, High nuclearity clusters containing methyl groups. Syntehsis and structures of pentaosmium-gold carbonyl cluster compounds, J. Organomet. Chem. 812 (2016) 108–114.

[23] C. Cesari, B. Berti, F. Calcagno, C. Femoni, M. Garavelli, M.C. Iapalucci, I. Rivalta, S. Zacchini, Polymerization isomerism in Co-M (M = Cu, Ag, Au) carbonyl clusters: synthesis, structures and computational investigation, Molecules 26 (2021) 1529.

[24] B. Berti, M. Bortoluzzi, C. Cesari, C. Femoni, M.C. Iapalucci, R. Mazzoni, F. Vacca, S. Zacchini, Thermal growth of Au-Fe heterometallic carbonyl clusters containing N-heterocyclic carbene and phosphine ligands, Inorg. Chem. 59 (2020) 2228–2240.

[25] B. Berti, M. Bortoluzzi, C. Cesari, C. Femoni, M.C. Iapalucci, L. Soleri, S. Zacchini, Synthesis, structural characterization, and DFT investigations of $[M_xM'_{5-x}Fe_4(CO)_{16}]^{3-}$ (M, M' = Cu, Ag, Au; M ≠ M') 2-D molecular alloy clusters, Inorg. Chem. 59 (2020) 15936–15952.

[26] I. Ciabatti, C. Femoni, M.C. Iapalucci, S. Ruggieri, S. Zacchini, The role of gold in transition metal carbonyl clusters, Coord. Chem. Rev. 355 (2018) 27–38.

[27] B. Berti, M. Bortoluzzi, C. Cesari, C. Femoni, M.C. Iapalucci, R. Mazzoni, F. Vacca, S. Zacchini, Polymerization isomerism in $[\{MFe(CO)_4\}_n]^{n-}$ (M = Cu, Ag, Au; n = 3, 4) molecular clusters supported by metallophilic interactions, Inorg. Chem. 58 (2019) 2911–2915.

[28] C. Cesari, M. Bortoluzzi, C. Femoni, M.C. Iapalucci, S. Zacchini, Mercurophilic interactions in heterometallic Ru-Hg carbonyl clusters, Inorg. Chim. Acta 545 (2023) 121281.

[29] F.A. Cotton, Transition-metal compounds containing clusters of metal atoms, Q. Rev. Chem. Soc. 20 (1966) 389–401.

[30] C. Cesari, J.-H. Shon, S. Zacchini, L.A. Berben, Metal carbonyl clusters of groups 8-10: synthesis and catalysis, Chem. Soc. Rev. 50 (2021) 9503–9539.

[31] C. Cesari, C. Femoni, F. Forti, M.C. Iapalucci, G. Scorzoni, S. Zacchini, Isomerism in molecular metal carbonyl clusters, Eur. J. Inorg. Chem. 27 (2024) e202400220.

[32] P.R. Raithby, The growth of higher nuclearity carbonyl clusters of ruthenium and osmium, J. Organomet. Chem. 1005 (2024) 122979.

[33] E.G. Mednikov, L.F. Dahl, Syntheses, structures and properties of primarily nanosized homo/heterometallic palladium CO/PR_3-ligated clusters, Phil. Trans. R. Soc. A 368 (2010) 1301–1332.

[34] C. Cesari, C. Femoni, F. Forti, M.C. Iapalucci, G. Scorzoni, S. Zacchini, Molecular hydride carbonyl clusters and nanoclusters, Inorg. Chim. Acta 574 (2025) 122394.

[35] C. Cesari, C. Femoni, M.C. Iapalucci, S. Zacchini, Molecular Fe, Co and Ni carbide carbonyl clusters and nanoclusters, Inorg. Chim. Acta. 544 (2023) 121235.

[36] G. Hogarth, S.E. Kabir, E. Nordlander, Cluster chemistry in the noughties: new developments and their relationship to nanoparticles, Dalton Trans. 39 (2010) 6153–6174.

[37] P. Buchwalter, J. Rosé, P. Braunstein, Multimetallic catalysis based on heterometallic complexes and clusters, Chem. Rev. 115 (2015) 28–126.

[38] R.D. Adams, B. Captain, Bimetallic cluster complexes: synthesis, structures and applications to catalysis, J. Organomet. Chem. 689 (2004) 4521–4529.

[39] R.D. Adams, M.D. Smith, J.D. Tedder, N.D. Wakdikar, Copper carbene complexes. Synthesis and structural analysis of a chloro-bridged dicopper cation and the triosmium-copper carbene cluster complex $HOs_3(CO)_{11}$ [μ-Cu(IPr)], J. Organomet. Chem. 941 (2021) 121799.

[40] R.D. Adams, P.J. Pellecchia, M.D. Smith, J.D. Tedder, N.D. Wakdikar, Heterometallic nitride cluster compounds: synthesis and characterizations of the first nitrido-containing ruthenium-gold and ruthenium-copper carbonyl cluster complexes, J. Organomet. Chem. 898 (2019) 120872.

[41] M.A. Beswick, J. Lewis, P.R. Raithby, M.C. Ramirez de Aurellano, The high nuclearity mixed-metal cluster dianions $[Ru_8H_2Cu_7Cl_3(CO)_{24}]^{2-}$ and $[Ru_{12}H_2Cu_6Cl_2(CO)_{34}]^{2-}$, Angew. Chem. Int. Ed. 36 (1997) 291–293.

[42] M. Shieh, C.-Y. Miu, K.J. Hsing, L.-F. Jang, C.-N. Lin, Copper-incorporated mono- and di-$TeRu_5$ metal carbonyl complexes: syntheses, structures, and an unusual skeletal arrangement, Dalton Trans. 44 (2015) 6526–6536.

[43] C. Cesari, M. Boroluzzi, C. Femoni, M.C. Iapalucci, S. Zacchini, One-pot atmospheric pressure synthesis of $[H_3Ru_4(CO)_{12}]^-$, Dalton Trans. 50 (2021) 9610–9622.

[44] C. Cesari, M. Bortoluzzi, F. Forti, L. Gubbels, C. Femoni, M.C. Iapalucci, S. Zacchini, 2-D molecular alloy Ru-M (M = Cu, Ag, and Au) carbonyl clusters: synthesis, molecular structure, catalysis, and computational studies, Inorg. Chem. 61 (2022) 14726–14741.

[45] M. Shieh, C.-C. Yu, Ternary copper-incorporated group 8 (Ru or Fe) carbonyl chalcogenide complexes and polymers: from syntheses to applications, J. Organomet. Chem. 849-850 (2017) 219–227.

[46] J.M. Thomas, R.D. Adams, E.M. Boswell, B. Captain, H. Grönbeck, R. Raja, Synthesis, characterization, electronic structure and catalytic performance of bimetallic and trimetallic nanoparticles containing tin, Faraday Discuss 138 (2008) 301–315.

[47] J.M. Thomas, B.F.G. Johnson, R. Raja, G. Sankar, P.A. Midgley, High-performance nanocatalysts for single-step hydrogenations, Acc. Chem. Res. 36 (2003) 20–30.

[48] M.I. Bruce, B.K. Nicholson, Cluster chemistry: XXIII. Mono-, di- and tri-auration of $H_4Ru_4(CO)_{12}$ with $[\{Au(PPh_3)\}_3O,BF_4]$: X-ray crystal structure of $HRu_4Au_3(CO)_{12}(PPh_3)_3$, J. Organomet. Chem. 252 (1983) 243–255.

[49] C. Cesari, M. Bortoluzzi, C. Femoni, F. Forti, M.C. Iapalucci, S. Zacchini, Peraurated ruthenium hydride carbonyl clusters: aurophilicity, isolobal analogy, structural isomerism, and fluxionality, Dalton Trans. 53 (2024) 3865–3879.

[50] M.I. Bruce, B.K. Nicholson, Cluster chemistry, Application of gold-oxonium reagents to the synthesis of poly-gold-mixed-metal clusters: preparation and X-ray crystal structure of $[Au_3CoRu_3(CO)_{12}(PPh_3)_3]$, containing a bicapped trigonal-bipyramidal metal cluster, J. Chem. Soc., Chem. Commun. (1982) 1141–1143.

[51] S. Grimme, A. Hansen, S. Ehlert, J.-M. Me, wes, r^2SCAN-3c: a "Swiss army knife" composite electronic-structure method, J. Chem. Phys. 154 (2021) 064103.

[52] R.P.B. Silalahi, H. Liang, Y. Jo, J.-H. Liao, T.-H. Chiu, Y.-Y. Wu, X. Wang, S. Kahlal, Q. Wang, W. Choi, D. Lee, J.-Y. Saillard, C.W. Liu, Hydride-containing Pt-doped Cu-rich nanoclusters: synthesis, structure, and electrocatalytic hydrogen evolution, Chem. Eur. J. 30 (2024) e202303755.

[53] R.P.B. Silalahi, H. Liang, M.N. Pillay, T.-H. Chiu, J.-H. Liao, S. Kahlal, J.-Y. Saillard, C.W. Liu, Structural alterations on copper cages containing hydrides coordinated to the central Pd (0), Inorg. Chim. Acta 568 (2024) 122071.

[54] M.S. Eberhart, J.R. Norton, A. Zuzek, W. Sattler, S. Ruccolo, Electron transfer from hexameric copper hydrides, J. Am. Chem. Soc. 135 (2013) 172621. -17265.

[55] M.J. Freeman, A.G. Orpen, I.D. Salter, The heteronuclear cluster chemistry of the Group 1B metals. Part 2. Synthesis, X-ray crystal structures, and dynamic behaviour of the bimetallic hexanuclear Group 1B metal cluster compounds

[$M_2Ru_4H_2(CO)_{12}(PPh_3)_2$] (M = Cu, Ag, or Au), J. Chem. Soc. Dalton Trans. (1987) 379–390.
[56] S.S.D. Brown, I.D. Salter, L. Troupet, The heteronuclear cluster chemistry of the Group 1B metals. Part 6. Synthesis, structures, and dynamic behaviour of the bimetallic hexanuclear Group 1B metal cluster compounds [$M_2Ru_4(\mu_3\text{-}H)_2\{\mu\text{-}Ph_2P(CH_2)_nPPh_2\}(CO)_{12}$] (M = Cu or Ag, n = 1-6). X-ray crystal structures of [$Cu_2Ru_4(\mu_3\text{-}H)_2\{\mu\text{-}Ph_2P(CH_2)_nPPh_2\}(CO)_{12}$] (n = 2, 5, or 5), J. Chem. Soc. Dalton Trans. (1988) 757–767.
[57] I.D. Salter, S.A. Williams, T. Adatia, The heteronuclear cluster chemistry of the group 1B metals-18. Synthesis, structural characterization and dynamic behviour of the bimetallic hexanuclear group 1B metal cluster compounds [$M_2Ru_4H_2(\mu\text{-}dppf)(CO)_{12}$,M = Cu, Ag, or Au; dppf = $Fe(\eta^5\text{-}C_5H_5PPh_2)_2$]. X-ray crystal structure of [$Cu_2Ru_4(\mu_3\text{-}H)_2(\mu\text{-}dppf)(CO)_{12}$], Polyhedron 14 (1995) 2803–2817.
[58] R.A. Brice, S.C. Pearse, I.D. Salter, K. Henrick, The heteronuclear cluster chemistry of the group 1B metals. Part 1. Structural similarities and differences among mixed-metal cluster compounds containing copper, silver, or gold atoms ligated by phosphines. X-ray crystal structures of [$CuRu_4(\mu_3\text{-}H)_3(CO)_{12}(PMePh_2)$] and [$CuRu_3(CO)_9(C_2Bu^t)(PPh_3)$], J. Chem. Soc. Dalton Trans. (1986) 2181–2192.
[59] T. Adatia, I.D. Salter, The heteronuclear cluster chemistry of the group 1B metals-19. X-ray crystal structure and dynamic behaviour in solution of the mixed-metal cluster [$\{CuRu_4(\mu_3\text{-}H)_3(CO)_{12}\}_2\{\mu\text{-}Ph_2P(CH_2)_2PPh_2\}$]: an investigation of the effect of a bidentate diphosphine ligand linking two cluster subunits, Polyhedron 15 (1996) 597–603.
[60] S.R. Parmelee, N.P. Mankad, A data-intensive re-evaluation of semibridging carbonyl ligands, Dalton Trans. 44 (2015) 17007–17014.
[61] C. Lepetit, P. Fau, K. Fajerwerg, M.L. Kahn, B. Silvi, Topological analysis of the metal-metal bond: a tutorial review, Coord. Chem. Rev. 345 (2017) 150–181.
[62] S. Dapprich, G. Frenking, Investigation of donor-acceptor interactions: a charge decomposition analysis using fragment molecular orbitals, J. Phys. Chem. 99 (1995) 9352–9362.
[63] F.L. Hirshfeld, Bonded-atom fragments for describing molecular charge densities, Theor. Chim. Acta (Berl.) 44 (1977) 129–138.
[64] M. Bortoluzzi, I. Ciabatti, C. Femoni, M. Hayatifar, M.C. Iapalucci, G. Longoni, S. Zacchini, Hydride migration from a triangular face to a tetrahedral cavity in tetranuclear iron carbonyl clusters upon coordination of $[AuPPh_3]^+$ fragments, Angew. Chem. Int. Ed. 53 (2014) 7233–7237.
[65] P.J. Bailey, M.A. Beswick, J. Lewis, P.R. Raithby, M.C. Ramirez de Arellano, Reactions of the hexaruthenium cluster anions $[Ru_6C(CO)_{16}]^{2-}$ and $[Ru_6(CO)_{18}]^{2-}$ with $Au_2\{ph_2PCH_2PPh_2\}Cl_2$: crystal and molecular structures of $Ru_6C(CO)_{16}Au_2\{ph_2PCH_2PPh_2\}$ and $Ru_5(CO)_{15}Au_2\{ph_2PCH_2PPh_2\}$, J. Organomet. Chem. 459 (1993) 293–301.
[66] M.R.A. Al-Mandhary, R. Buntem, C.L. Doherty, A.J. Edwards, J.F. Gallagher, J. Lewis, C.-K. Li, P.R. Raithby, M.C. Ramirez de Arellano, G.P. Shields, Ise of the cationic fragments $[Ru(\eta^5\text{-}C_5H_5)(MeCN)_3]^+$ and $[M(\eta^6\text{-}C_6H_5R)(MeCN)_3]^+$ (M = Os, Ru; R = H, Me) as ionic coupling reagents in the synthesis of the clusters $[Os_4M_2(CO)_{12}(\eta^6\text{-}C_6H_5R),Os_4M(CO)_{12}(\eta^6\text{-}C_6H_6)(Au_2dppm)]$ and $[Os_5Ru(CO)_{15}(\eta^5\text{-}C_5H_5)(AuPPh_3)]$, J. Clust. Sci. 16 (2005) 127–150.
[67] C. Femoni, M.C. Iapalucci, G. Longoni, S. Zacchini, The chemistry of hydridocarbonylferrates revisited: syntheses and structures of the new $[H_2Fe_4(CO)_{12}]^{2-}$ and $[HFe_5(CO)_{14}]^{3-}$ anions, and the $[Fe(DMF)_4,Fe_4(CO)_{12}(\mu_5\text{-}\eta^2\text{-}CO)(\mu\text{-}H)]_2$ adduct containing an unprecedented isocarbonyl, Dalton Trans. 40 (2011) 8685–8964.
[68] J.J. Guy, G.M. Sheldrick, Bis(triphenylsphosphine)iminium μ-hydrido-pentadeacarbonylpentaosmate, $[(Ph_3P)_2N]^+[HOs_5(CO)_{15}]^-$, Acta Cryst. B34 (1978) 1722–1725.
[69] A.V. Rivera, G.M. Sheldrick, M.B. Hursthouse, Bis(triphenylphosphine)iminium pentadecacarbonyliodopentaosmate, Acta Cryst. B34 (1978) 3376–3379.
[70] B.E. Reichert, G.M. Sheldrick, Hexadecacarbonylpentaosmium, Acta Cryst. B33 (1977) 173–175.
[71] B.F. Johnson, J. Lewis, W.J.H. Nelson, M.A. Pearsall, P.R. Raithby, M.J. Rosales, M. McPartlin, A. Sironi, Reactions of $[Os_5H_2(CO)_{15}]$ with pyridine: crystal and molecular structures of $[Os_5H_3(CO)_{14}(C_5H_4N)]$ and $[Os_5H_2(CO)_{14}(C_5H_5N)]$, J. Chem. Soc. Dalton Trans. (1987) 327–333.
[72] W. Wang, F.W.B. Einstein, R.K. Pomeroy, Site preference of the *tert*-butyl isocyanide ligand in pentaosmium carbonyl clusters. Crystal structures of $Os_5(CO)_{18}(CNBu^t)$ and $Os_5(CO)_{15}(CNBu^t)$, Organomet 13 (1994) 1114–1119.
[73] D.A. McCarthy, J.A. Krause, S.G. Shore, Formation and characterization of an 84-electron hexaruthenium cluster: spontaneous decarbonylation of $H_2Ru_6(CO)_{18}$ to form $H_2Ru_6(CO)_{17}$, J. Am. Chem. Soc. 112 (1990) 8587–8589.
[74] B. Berti, M. Bortoluzzi, C. Cesari, C. Femoni, M. Hayatifar, M.C. Iapalucci, S. Zacchini, Bimetallic Fe-Ir and trimetallic Fe-Ir-Au carbonyl clusters containing hydride and/or phosphine ligands: syntheses, structures and DFT studies, J. Clust. Sci. 32 (2021) 743–753.
[75] A. Bondi, van der Waals volumes and radii, J. Phys. Chem. A 68 (1964) 441–451.
[76] E. Wiberg, A.F. Holleman, N. Wiberg, Lehrbuch Der Anorganischen Chemie, 102nd ed, de Gruyter, Berlin, 2007.
[77] B. Berti, M. Bortoluzzi, C. Cesari, C. Femoni, M.C. Iapalucci, R. Mazzoni, S. Zacchini, A comparative experimental and computational study of heterometallic Fe-M (M = Cu, Ag, Au) carbonyl clusters containing N-heterocyclic carbene ligands, Eur. J. Inorg. Chem. (2020) 2191–2202.
[78] M. Bortoluzzi, I. Ciabatti, C. Cesari, C. Femoni, M.C. Iapalucci, S. Zacchini, Synthesis of the highly reduced $[Fe_6C(CO)_{15}]^{4-}$ carbonyl carbide cluster and its reactions with H^+ and $[Au(PPh_3)]^+$, Eur. J. Inorg. Chem. (2017) 3135–3143.
[79] M. Bortoluzzi, C. Cesari, I. Ciabatti, C. Femoni, M. Hayatifar, M.C. Iapalucci, R. Mazzoni, S. Zacchini, Bimetallic Fe-Au carbonyl clusters derived from Collman's reagent: synthesis, structure and DFT analysis of Fe(CO) $(_4(AuNHC)_2$ and $[Au_3Fe_2(CO)_8(NHC)_2]$, J. Clust. Sci. 28 (2017) 703–723.
[80] C. Femoni, B. Berti, F. Calcagno, C. Lucarelli, M. Garavelli, R. Mazzoni, I. Rivalta, S. Zacchini, Bimetallic Co-M (M = Cu, Ag, Au) carbonyl complexes supported by N-heterocyclic carbene ligands: synthesis, structures, computational investigation, and catalysis for ammonia borane dehydrogenation, Organometallics 40 (2021) 2724–2735.
[81] C. Cesari, M. Bortoluzzi, C. Femoni, M.C. Iapalucci, S. Zacchini, Synthesis, molecular structure and fluxional behavior of the elusive $[HRu_4(CO)_{12}]^{3-}$ carbonyl anion, Dalton Trans. 51 (2022) 2250–2261.
[82] C.F. Macrae, I. Sovago, S.J. Cottrell, P.T.A. Galek, P. McCabe, E. Pidcock, M. Platings, G.P. Shields, J.S. Stevens, M. Towler, P.A. Wood, Mercury4.0: from visualization to analysis, design and prediction, J. Appl. Crystallogr. 53 (2020) 226–235.
[83] G.M. Sheldrick, SADABS-2008/1-Bruker AXS Area Detector Scaling and Absorption Correction, Bruker AXS, Madison, WI, 2008.
[84] G.M. Sheldrick, Crystal structure refinement with SHELXL, Acta Crystallogr. Sect. C Struct. Chem. 71 (2015) 3–8.
[85] J.W. Furness, A.D. Kaplan, J. Ning, J.P. Perdew, J. Sun, Accurate and numerically efficient r^2SCAN meta-generalized gradient approximation, J. Phys. Chem. Lett. 11 (2020) 8208–8215.
[86] H. Kruse, S. Grimme, A geometrical correction for the inter-and intra-molecular basis set superposition error in Hartree-Fock and density functional theory calculations for large systems, J. Chem. Phys. 136 (2012) 154101.
[87] E. Caldeweyher, S. Ehlert, A. Hansen, H. Neugebauer, S. Spicher, C. Bannwarth, S. Grimme, A generally applicable atomic-charge dependent London dispersion correction, J. Chem. Phys. 150 (2019) 154122.
[88] F. Neese, Software update: the ORCA program system - Version 5.0, WIREs Comput. Mol. Sci. 12 (2022) e1616.
[89] T. Lu, A comprehensive electron wavefunction analysis toolbox for chemists, Multiwfn, J. Chem. Phys. 161 (2024) 082503.
[90] J.P. Perdew, A. Ruzsinszky, G.I. Csonka, O.A. Vydrov, G.E. Scuseria, L. A. Constantin, X. Zhou, K. Burke, Restoring the density-gradient expansion for exchange in solids and surfaces, Phys. Rev. Lett. 100 (2008) 136406.
[91] J.S. Lin, A. Qteish, M.C. Payne, V. Heine, Optimized and transferable nonlocal separable ab initio pseudopotentials, Phys. Rev. B 47 (1993) 4174–4180.
[92] A. Tkatchenko, M. Scheffler, Accurate molecular Van Der Waals interactions from ground-State electron density and free-atom reference data, Phys. Rev. Lett. 102 (2009) 073005.
[93] D.D. Koelling, B.N. Harmon, A technique for relativistic spin-polarised calculations, J. Phys. C Solid State Phys. 10 (1977) 3107–3114.
[94] S.J. Clark, M.D. Segall, C.J. Pickard, P.J. Hasnip, M.I.J. Probert, K. Refson, M. C. Payne, First principles methods using CASTEP.Z, Kristallogr 220 (2005) 567–570.